For resubmission to *Environmental microbiology* (EMI-2022-0180)

Growth of nitrite-oxidizing *Nitrospira* and ammonia-oxidizing *Nitrosomonas* in marine recirculating trickling biofilter reactors

Mamoru Oshiki[1, 2*], Hirotoshi Netsu[2, 3], Kyohei Kuroda[4], Takashi Narihiro[4], Naoki Fujii[5], Tomonori Kindaichi[5], Yoshiyuki Suzuki[2], Takashiro Watari[3], Masashi Hatamoto[3], Takashi Yamaguchi[6], Nobuo Araki[2] & Satoshi Okabe[1]

[1] Division of Environmental Engineering, Faculty of Engineering, Hokkaido University, North 13, West 8, Kita-ku, Sapporo, Hokkaido 060-8628, Japan

[2] Department of Civil Engineering, National Institute of Technology, Nagaoka College, 888 Nishikatakaimachi, Nagaoka, Niigata 940-8532, Japan.

[3] Department of Environmental Systems Engineering, Nagaoka University of Technology, 1603-1 Kamitomioka, Nagaoka, Niigata 940-2188, Japan.

[4] Bioproduction Research Institute, National Institute of Advanced Industrial Science and Technology (AIST), 2-17-2-1 Tsukisamu-Higashi, Toyohira-ku, Sapporo, Hokkaido, 062-8517 Japan

[5] Department of Civil and Environmental Engineering, Graduate School of Engineering, Hiroshima University, 1-4-1 Kagamiyama, Higashihiroshima, Hiroshima 739-8527, Japan

[6] Department of Science of Technology Innovation, Nagaoka University of Technology, 1603-1 Kamitomioka, Nagaoka, Niigata 940-2188, Japan.

These authors contributed equally: Mamoru Oshiki, Hirotoshi Netsu, Kyouhei Kuroda

Article type: Research article

Running title: Growth of nitrifiers in trickling filter reactors

Declarations of interest: none

[*]**Corresponding author:**

Mamoru Oshiki (Ph.D.)

E-mail; oshiki@eng.hokudai.ac.jp

Tel/Fax; +81-11-706-7597/7162

31 **Originality-significance statement**

32 Aerobic nitrite oxidation (NO_2^- to NO_3^-) yields much less Gibbs free energy than aerobic

33 ammonia oxidation (NH_3 to NO_2^-), while dominance of nitrite-oxidizing bacteria (NOB) over

34 ammonia-oxidizing bacteria (AOB) has been found in marine recirculating trickling biofilter

35 reactors. Specific mechanism responsible for the formation of this puzzling microbial

36 community has not been explored in detail, and the present study shed light on this subject.

37 The present study shows novel ecological aspects of nitrite-oxidizing *Nitrospira* and

38 ammonia-oxidizing *Nitrosomonas* proliferated in trickling biofilter reactors.

Summary (190 words)

Aerobic ammonia and nitrite oxidation reactions are fundamental biogeochemical reactions contributing to the global nitrogen cycle. Although aerobic nitrite oxidation yields 4.8-folds less Gibbs free energy (ΔG_r) than aerobic ammonia oxidation in the NH_4^+-feeding marine recirculating trickling biofilter rectors operated in the present study, nitrite-oxidizing and not ammonia-oxidizing *Nitrospira* (sublineage IV) outnumbered ammonia-oxidizing *Nitrosomona*s (relative abundance; 53.8% and 7.59%, respectively). CO_2 assimilation efficiencies during ammonia or nitrite oxidation were 0.077 μmol-$^{14}CO_2$/μmol-NH_3 and 0.053 to 0.054 μmol-$^{14}CO_2$/μmol-NO_2^-, respectively, and the difference between ammonia and nitrite oxidation was much smaller than the difference of ΔG_r. Free-energy efficiency of nitrite oxidation was higher than ammonia oxidation (31-32% and 13%, respectively), and high CO_2 assimilation and free-energy efficiencies were a determinant for the dominance of *Nitrospira* over *Nitrosomonas*. Washout of *Nitrospira* and *Nitrosomonas* from the trickling biofilter reactors was also examined by quantitative PCR assay. Normalized copy numbers of *Nitrosomonas amoA* was 1.5- to 1.7-folds greater than *Nitrospira nxrB* and 16S rRNA gene in the reactor effluents. *Nitrosomonas* was more susceptible for washout than *Nitrospira* in the trickling biofilter reactors, which was another determinant for the dominance of *Nitrospira* in the trickling biofilter reactors.

57 **Introduction**

58 Nitrification is a key microbial process in the global nitrogen cycle and also for biological
59 nitrogen removal from wastewater. In the nitrification process, ammonia is aerobically
60 oxidized to nitrite by aerobic ammonia-oxidizing bacteria and archaea (AOB and AOA,
61 respectively), and the formed nitrite is subsequently oxidized to nitrate by aerobic nitrite-
62 oxidizing bacteria (NOB). Phylogenetically diverse NOB such as *Nitrospira* (phylum
63 *Nitrospirota*), *Nitrospina* (*Nitrospinota*), *Nitrobacter*, *Nitrotoga*, *Nitrococcus*
64 (*Proteobacteria*), *Nitrolancea* (*Chloroflexota*) have been identified by culture-dependent and
65 -independent techniques (Daims *et al*., 2016). The genus *Nitrospira* consists of
66 phylogenetically diverse members (*i.e.*, at least six phylogenetic sublineages) (Lebedeva *et*
67 *al*., 2011), and *Nitrospira* population has been found from wide range of man-made and
68 natural ecosystems (Daims *et al.*, 2016). Additionally, the members of the *Nitrospira*
69 sublineage II has a unique metabolic capability, complete ammonia oxidation (commamox),
70 and commamox *Nitrospira* oxidize ammonia to nitrate via nitrite in a single cell (Daims *et al.*,
71 2015; van Kessel *et al.*, 2015). Population of commamox *Nitrospira* has been found in
72 freshwater and groundwater ecosystems, but rarely found in marine environments (Xia *et al.*,
73 2018).

74 Thermodynamically, aerobic ammonia oxidation yields larger Gibbs free energy than
75 aerobic nitrite oxidation; therefore, numerical dominance of AOB and/or AOA over NOB is

76 expected where nitrification proceeds. Indeed, stoichiometric and thermodynamic calculation
77 of nitrification processes has enabled to approximate population size and growth yields of
78 AOA and NOB in ocean (Zakem *et al.*, 2018; Zhang *et al.*, 2020). On the other hand,
79 numerical dominance of *Nitrospira* over AOA/AOB has been described in the recirculating
80 trickling filter reactors operated for marine aquacultures (Foesel *et al.,* 2008; Keuter *et al.,*
81 2011; 2017; Brown *et al.,* 2013). Another example is our previous study (Oshiki *et al.*, 2020),
82 where *Nitrospira* outnumbered AOB and AOA in NH_4^+-feeding marine recirculating trickling
83 filter reactors (down-hanging sponge, DHS, reactors); 55%, 10% and <0.1% of total biomass,
84 respectively. Numerical dominance of *Nitrospira* over AOB/AOA in the DHS reactors was
85 somewhat surprising because the ΔG_r of aerobic ammonia oxidation was 4.8-folds higher in
86 the NH_4^+-feeding DHS reactor than that of aerobic nitrite oxidation (**Supplementary text 1**).
87 However, the mechanism(s) responsible for the dominance of *Nitrospira* over AOB and AOA
88 in marine trickling filter reactors has not been explored in detail.
89 Consequently, the present study aimed to examine how *Nitrospira* outnumbered the
90 population of AOB (*i.e.*, *Nitrosomonas*) in the DHS reactors. The two DHS reactors were
91 operated with feeding of the inorganic seawater media containing NH_4^+ or NO_2^- (designated
92 as NH_4^+- and NO_2^--feeding DHS reactors, respectively) at 20ºC, and metagenomic analyses
93 using the biomass retained in the reactors were performed to examine metabolic potentials of
94 *Nitrospira* and *Nitrosomonas*. Because genomic data only suggested metabolic potential, a

95 series of batch incubations were performed to examine CO_2 assimilation efficiencies, free-
96 energy efficiencies, and H_2 oxidation activity. CO_2 assimilation efficiencies were determined
97 by examining $^{14}CO_2$ incorporation into the biomass, and this approach has been used for
98 determining the yields of carbon fixation by nitrifiers (Glover *et al*., 1985; Tsai and Tuovinen
99 1986; Bayer *et al.*, 2022) and for the biomass yields of anaerobic ammonia oxidizing bacteria
100 (Ali *et al*., 2015; Awata *et al.*, 2015). Apart from the above metagenomic and physiological
101 experiments, washout of *Nitrosomonas* and *Nitrospira* in the NH_4^+-feeding DHS reactor was
102 examined by determining the copy number of AOB *amoA*, *Nitrospira nxrB*, and *Nitrospira*
103 16S rRNA gene in the reactor effluents by quantitative PCR (qPCR) assay.
104

105 **Results**

106 ***Metagenomic analysis of NH_4^+- and NO_2^--enriched biomass***

107 NH_4^+- and NO_2^--feeding DHS reactors were operated continuously for more than 1 y without

108 disturbances, and *Nitrospira* proliferated as a dominant population in both the operated

109 reactors as examined by fluorescence *in-situ* hybridization (**Fig. 1**). Metagenomic analyses

110 using the biomass collected from the NH_4^+- or NO_2^--feeding DHS reactors (designated as the

111 NH_4^+- or NO_2^--enriched biomass, respectively) were performed, and the 35.4 and 52.8 M

112 reads of 200-bp paired-end reads corresponding to 14.2 and 21.1 Gb were obtained from the

113 NH_4^+- and NO_2^--enriched biomass, respectively. Those sequence reads were assembled into

114 30 bacterial bins, which contained the 6 *Nitrospira* (NPIRA01 to NPIRA06 bins) and 2

115 *Nitrosomonas* (NMNS01 and NMNS02 bins) bins (**Table 1**).

116 Relative abundances and phylogeny of the obtained 30 bins were shown in **Table 1**

117 and **Fig. S1**, respectively. The relative abundances of the *Nitrospira* (especially, the

118 NPIRA01, NPIRA02, NPIRA04 bins) and *Nitrosomonas* bins (the NMNS02 bin) were much

119 higher than the other bins, indicating that *Nitrospira* and *Nitrosomonas* were the predominant

120 bacteria in the NH_4^+- and/or NO_2^--enriched biomass. Especially, the sum of the relative

121 abundances of the NPIRA bins were 53.8% and 72.2% in the NH_4^+- and NO_2^--enriched

122 biomass, indicating *Nitrospira* was highly abundant in both the biomass. As for *Nitrosomonas*

123 bins, the sum of the relative abundances of the NMSN bins were 7.59% and 0.62% in the

124 NH_4^+- and NO_2^--enriched biomass (**Table 1**), indicating *Nitrospira* outnumbered

125 *Nitrosomonas* in both the DHS reactors.

126 ***Phylogeny and metabolic potential of NPIRA bins***

127 The NPIRA bins were affiliated into the *Nitrospira* sublineage IV (Lebedeva *et al.,* 2011)

128 (**Fig. 2**). The average nucleotide identity (ANI) values among the NPIRA bins were 71−89%

129 (**Table S1**), indicating each NPIRA bins represented different *Nitrospira* species (Richter and

130 Rosselló-Móra, 2006). The NPIRA03 and NPIRA06 bins were affiliated into the *Nitrospira*

131 *marina* clade including *Nitrospira marina*, a mesophilic and halophilic nitrite oxidizing

132 bacterium. Other NPIRA bins were affiliated into a phylogenetically-different clade in which

133 closely-relating *Nitrospira* genome was not available in public database (accessed on Jan.

134 2021). Phylogenetic affiliation of this clade was examined using the 16S rRNA gene sequence

135 located in the NPIRA02 bin (the NPIRA02_r00020 gene). The NPIRA02_r00020 gene

136 showed the 97.5% identity with the partial 16S rRNA gene sequences of *Candidatus*

137 *Nitrospira salsa* clone Cb18 (accession number KC706459.1) (**Fig. S2**), and this clade was

138 tentatively designated as the *Nitrospira salsa* clade in the present study. The NPIRA01,

139 NPIRA02, and NPIRA04 bins affiliated into the *Nitrospira salsa* clade were dominant

140 *Nitrospira* (*i.e.*, >10% of relative abundance in a biomass) both in the NH_4^+- or NO_2^--feeding

141 DHS reactors (**Table 1**).

142 Metabolic potential of the NPIRA bins was investigated by examining presence and
143 absence of functional genes (**Table S2**). The genes required for nitrite oxidation
144 (nitrite:nitrate oxidoreductase, *nxr*), energy conservation (cytochrome *bd*-like heme-copper
145 terminal oxidase), NAD(P)H generation (complex I), and CO_2 fixation through the rTCA
146 cycle (2-oxoglutarate:ferredoxin oxidoreductase, OGOR, five- or four-subunit
147 pyruvate:ferredoxin oxidoreductase, POR, and ATP-citrate lyase, ACL) were conserved in the
148 NPIRA bins (a full description is available as **supplemental text 2)**. On the other hand,
149 orthologues of commamox *Nitrospira amoCAB* (threshold *e*-value of blastp search 10^{-15}) were
150 not found in the NPIRA bins and also in the other known *Nitrospira* sublineage IV genomes.
151 The orthologue of commamox *Nitrospira hao* was also missing in the NPIRA bins and the
152 *Nitrospira* sublineage IV genomes, whereas the orthologue encoding octaheme cytochrome *c*
153 (a phylogenetically-relevant protein with Hao) (Bergmann *et al*., 2005) found in the canonical
154 NO_2^--oxidizing *Nitrospira* genomes (*Nitrospira moscoviensis* and *Nitrospira japonica*
155 genomes) was located in the NPIRA2 and NPIRA3 bins (**supplemental text 2** and **Table S3**).
156 *Nitrospira* bacteria are metabolically versatile bacteria, and hydrogenotrophic growth
157 of *Nitrospira moscoviensis* (Koch *et al.*; 2014) has been demonstrated. The genes required for
158 H_2 oxidation and also degradations of carbohydrate and protein were conserved in the NPIRA
159 bins. A *hyd* gene cluster encoding a Group 3b NiFe hydrogenase and accessory proteins
160 required for the maturation of the NiFe hydrogenase was conserved in the NPIRA03 and

161 NPIRA04 bins (**Table S2**). On the other hand, the genes encoding putative Group 2a NiFe
162 hydrogenase (HupSL) were located in the NPIRA01 and NPIRA04 bins; therefore, the
163 NPIRA04 bin had both the Group 3b and Group 2a NiFe hydrogenase as previously found in
164 *Ca. Nitrospira alkalitolerans* (Daebeler *et al.*, 2020). The NPIRA03 and NPIRA06 bins had
165 the gene encoding formate dehydrogenase (Fdh) involved in formate oxidation. *Nitrospira*
166 *marina* cells can grow chemoorganotrophically on formate even without nitrite (Bayer et al.,
167 2021), and the NPIRA03_20570 and NPIRA06_25420 proteins showed 91.44 and 91.59%
168 identities with *Nitrospira marina* Fdh (the NMARINA_v1_1399 protein). On the other hand,
169 the *fdh* was not found in the NPIRA bins affiliated to *Nitrospira salsa* clade. The genes
170 encoding the enzymes involved in the degradation of carbohydrate (glycoside hydrolase, *β*-
171 glucosidase A, and alpha-amylase) and protein (secreted peptidases) were conserved in the
172 NPIRA03, NPIRA04, and NPIRA06 bins. As for the uptake of carbohydrate, amino acid and
173 peptides, ABC transporters for amino acid, oligo- and dipeptides were found in the NPIRA
174 bins whereas the sugar transporters were only found in specific NPIRA bins. The genes
175 encoding sugar ABC transporter were located in the NPIRA04 bin, whereas putative
176 carbohydrate-selective porin was found from NPIRA01, NPIRA02 and NPIRA03 bins.

177 ***Phylogeny and metabolic potential of NMNS bins***

178 The NMNS01 and NMNS02 bins were affiliated into the *Nitrosomonas* sp. Nm143 and
179 *Nitrosomonas aestuarii/marina* clades, respectively (**Fig. 3**), and the members of

180 *Nitrosomonas* sp. Nm143 and *Nitrosomonas aestuarii* were previously found in recirculating

181 marine aquaculture systems (Itoi *et al.*, 2006; Foesel *et al.*, 2008). The genes required for

182 aerobic ammonia oxidation and energy conservation (*amo*, *hao*, complex III and terminal

183 oxidase) and for NAD(P)H generation (*i.e.*, reverse electron transport) were generally

184 conserved in the NMNS01 and NMNS02 bins (See **Supplemental text 2** for details.).

185 Orthologue of *amo* was not found from the obtained bins other than NMNS01 and NMNS02

186 bins. The NMNS bins had the genes encoding ribulose-1,5-bisphosphate carboxylase

187 (RuBisCO) and ribuose-5-phosphate kinase (**Table S4**), suggesting that those *Nitrosomonas*

188 fixed CO_2 using the Calvin-Benson cycle. It was previously shown that *Nitrosomonas* was

189 capable of H_2 oxidation coupled with nitrite reduction (Bock *et al.*, 1995), and the NMNS

190 bins had the genes encoding putative NiFe hydrogenase and accessory proteins (*i.e.*, Group 3b

191 and Group 3d NiFe hydrogenase for the NMNS01 and NMNS02 bins, respectively) (**Table**

192 **S4**). Those genes were not located as a single gene cluster but found as multiple gene clusters

193 as previously found in the *Nitrosomonas oligotropha* genome (Sedlacek *et al.*, 2019).

194 ***Cultivation-dependent characterization of NH_4^+- and NO_2^--enriched biomass***

195 ***CO_2 assimilation and free-energy efficiencies during aerobic ammonia or nitrite oxidation***

196 $^{14}CO_2$ assimilation into the NH_4^+- and NO_2^--enriched biomass during aerobic ammonia and

197 nitrite oxidation was examined by incubating the biomass with the addition of 0.5 mM

198 NH_4^+or NO_2^- and ^{14}C-labeled sodium bicarbonate. The NH_4^+-enriched biomass consumed

199 both $NH_4^+$and NO_2^-, and produced NO_3^- stoichiometrically (**Fig. 4, left**). During the ammonia

200 and nitrite oxidation, $^{14}CO_2$ was assimilated into the NH_4^+-enriched biomass, and the CO_2

201 assimilation efficiencies were determined to be 0.13 ± 0.019 (mean ± standard deviation

202 derived from triplicate incubation) μmol-CO_2/μmol-NH_3 and 0.053 ± 0.013 μmol-CO_2/μmol-

203 NO_2^-, respectively (**Table 2**). It is notable that autotrophic bacteria release a part of fixed CO_2

204 as dissolved organic carbon (DOC) (Oshiki *et al*., 2011), and the determined $^{14}CO_2$

205 assimilation does not include the fraction of DOC; *e.g.*, approx. 6-8% and 12% of fixed CO_2

206 were released as DOC in the culture of marine *Nitrosomonas* and *Nitrospira marina* Nb-295,

207 respectively (Bayer *et al*., 2022). No $^{14}CO_2$ assimilation was detected from the pasteurized

208 biomass and the biomass incubated without the addition of NH_4^+ or NO_2^-. The CO_2

209 assimilation efficiency of the ammonia oxidation reaction could not be determined directly

210 because the formed NO_2^- was subsequently oxidized to NO_3^- without the accumulation of

211 NO_2^- (**Fig. 4, left**). Therefore, the CO_2 assimilation efficiency of the ammonia oxidation was

212 approximated by subtracting the CO_2 assimilation efficiency of ammonia oxidation reaction

213 with that of nitrite oxidation reaction (*i.e*., 0.13 μmol-CO_2/μmol-NH_3 and 0.053 μmol-

214 CO_2/μmol-NO_2^-, respectively), which was 0.077 μmol-CO_2/ μmol-NH_3.

215 As for the NO_2^--enriched biomass, the biomass consumed NO_2^- and

216 stoichiometrically produced NO_3^- (**Fig. 4, right**). On the other hand, the NO_2^--enriched

217 biomass did not consume NH_4^+, and no$^{14}CO_2$ assimilation was found. The CO_2 assimilation

218 efficiency of the nitrite oxidation reaction was determined to be 0.054 ± 0.019 μmol-

219 CO_2/μmol-NO_2^-, which was the same with that determined using the NH_4^+-enriched biomass

220 (*i.e.*, 0.053 ± 0.013 μmol-CO_2/μmol-NO_2^-).

221 Free-energy efficiencies during the ammonia and nitrite oxidation were calculated

222 from the obtained CO_2 assimilation efficiencies (see the section Experimental procedures for

223 the calculation of the efficiencies), and compared with those previously determined using

224 AOB and NOB cultures (**Table 2**). The CO_2 assimilation and free-energy efficiencies of the

225 ammonia oxidation reaction obtained in the present study (*i.e.*, 0.077 μmol-CO_2/μmol-NH_3

226 and 13%, respectively) were comparable with those previously determined from AOB

227 cultures. As for the CO_2 assimilation and free-energy efficiencies of the nitrite oxidation

228 reaction, those obtained in the present study (*i.e.*, 0.053 to 0.054 μmol-CO_2/μmol- NO_2^- and

229 31 to 32%, respectively) were greater than those previously determined from NOB including

230 *Nitrospira marina* Nb-295 (Bayer *et al*., 2022). The 31 - 32% of the free-energy efficiencies

231 of the nitrite oxidation was >2.3-fold higher than that of ammonia oxidation reaction (*i.e.*,

232 13%).

233 ***Activities of H_2 oxidation***

234 The above metagenomic analysis suggested that *Nitrospira* sp. NPIRA03, NPIRA01 and

235 NPIRA04 and *Nitrosomonas* sp. NSMS01 and NSMS02 were capable of H_2 oxidation, and

236 the activities of the H_2 oxidation of NH_4^+- and NO_2^--enriched biomass were examined by

237 performing batch incubations. It should be noted that the genes encoding putative NiFe

238 hydrogenase were also found from the bins other than NPIRA and NSMS bins (*i.e.*,

239 DHS20C07, DHS20C08, DHS20C16, DHS20C18, and DHS20C20 bins). Involvement of

240 those bacteria to H_2 oxidation could not be ruled out here, while the abundance of those bins

241 was much less than *Nitrospira* bins (**Table 1**). Although both the NH_4^+- and NO_2^--enriched

242 biomass showed the activities of H_2 oxidation, the activities appeared after 4 d of incubation

243 (**Fig. 5**). Occurrence of the lag phase indicated that H_2 oxidation was not an active metabolic

244 pathway in the NH_4^+- and NO_2^--enriched biomass at least in the operated DHS reactors. This

245 conclusion agreed with the observation obtained from the batch incubation in which the

246 NH_4^+- and NO_2^--enriched biomass were incubated with the addition of $^{14}CO_2$ and H_2. The

247 NH_4^+- and NO_2^--enriched biomass were incubated for 18 h (*i.e.*, within the above lag phase),

248 and no $^{14}CO_2$ assimilation was found in both the biomass during the 18 h of incubation.

249 ***Washout of Nitrospira and Nitrosomonas from the NH_4^+-feeding DHS reactor***

250 Washout of *Nitrospira* and *Nitrosomonas* cells from the NH_4^+-feeding DHS reactor

251 were examined by determining the copy number of AOB *amoA*, *Nitrospira nxrB* and

252 *Nitrospira* 16S rRNA gene in reactor effluents. For the purpose, the qPCR assays of AOB

253 *amoA*, *Nitrospira nxrB* and *Nitrospira* 16S rRNA gene were carried out. There was a linear

254 relationship between the log copy number of standard DNAs and threshold cycle values (C_t

255 value) (R^2 >0.995), and efficiencies of PCR amplification were 1.83 to 2.02. As shown in **Fig.**

256 **6**, all the AOB *amoA*, *Nitrospira nxrB* and *Nitrospira* 16S rRNA gene were detected from the

257 effluents, indicating both *Nitrosomonas* and *Nitrospira* were detached and washed out from

258 the NH_4^+-feeding DHS reactor. The ratio of the copy numbers of AOB *amoA* to *Nitrospira*

259 *nxrB* and *Nitrospira* 16S rRNA gene increased in the effluents. Especially, *Nitrospira* 16S

260 rRNA gene was less abundant than AOB *amoA* in the effluents, indicating larger amounts of

261 *Nitrosomonas* population was washed out from the NH_4^+-feeding DHS reactor.

262 ***Discussion***

263 *Nitrospira* bacteria affiliated into the *Nitrospira salsa* or *Nitrospira marina* clade were

264 enriched in the NH_4^+- and NO_2^--feeding DHS reactors, and those *Nitrospira* outnumbered the

265 population of *Nitrosomonas* both in the DHS reactors. Those *Nitrospira* enriched in the DHS

266 reactors were most likely canonical nitrite-oxidizing *Nitrospira* because 1) the NPIRA bins

267 and the known *Nitrospira* sublineage IV genomes did not have the orthologue of *amoCAB*

268 and *hao* and 2) the *Nitrospira* of the NO_2^--enriched biomass did not show the activity of

269 aerobic ammonia oxidation (**Fig. 4**) although they (*i.e.*, the NPIRA01 to NPIRA06) were

270 commonly found in the NH_4^+- and NO_2^--enriched biomass. Additionally, commamox

271 *Nitrospira* (affiliated into the *Nitrospira* sublineage II) has been found from freshwater and

272 groundwater ecosystems (Xia *et al.*, 2018), whereas no commamox *Nitrospira* has been

273 recognized from the *Nitrospira* sublineage IV often found in saline environments (Daims *et*

274 *al.*, 2016; Park *et al.*, 2020). It is obvious to raise the question of how *Nitrospira* sp.

275 NPIRA02 and NPIRA04 outnumbered *Nitrosomonas* sp. NMNS01 and NMNS02 in the

276 NH_4^+-feeding DHS reactor. Not only the present study, the previous studies have also

277 indicated *Nitrospira* sublineage IV population outnumbered the population of aerobic

278 ammonia oxidizers in marine aquaculture systems (**Table S5**) (Foesel *et al.*, 2008; Keuter *et*

279 *al.*, 2011; 2017; Brown *et al.*, 2013).

280 Aerobic ammonia oxidation reaction yields 4.8-times higher free energy than NO_2^-

281 oxidation reaction in the NH_4^+-feeding DHS reactor. However, the free energy recovered

282 from the ammonia oxidation reaction must be much lower than the ΔG_r due to the following

283 reasons. First, there is no evidence that the first reaction of aerobic ammonia oxidation to

284 NH_2OH involves translocation of H^+ and formation of proton motive force (Costa *et al.*, 2006;

285 Simon and Klotz, 2013). The reaction of aerobic ammonia oxidation to NH_2OH is a

286 monooxygenation reaction catalyzed by Amo (Lancaster *et al.*, 2018), and the free energy

287 released during monooxygenation reactions (more specifically, O_2 reduction reaction) are not

288 conserved and dissipated (VanBriesen, 2001). Dissipation of the free energy during the

289 monooxygenation reaction of CH_4 (Yuan and VanBriesen, 2002) and NH_3 (Hollocher *et al.*,

290 1982) has been described, and both the reactions are catalyzed phylogenetically relevant

291 monooxygenase (i.e., Pmo and Amo, respectively). Indeed, *Nitrosomonas europaea* cells

292 showed nearly same effective H^+/O ratios during aerobic ammonia and NH_2OH oxidation

293 (*i.e.*, 4.1 and 3.9 of effective H^+/O ratios, respectively) (Hollocher *et al.*, 1982), indicating the

294 contribution of the reaction of ammonia oxidation to NH_2OH to the translocation of H^+ is

295 minor. The $\Delta G_r'^o$ for the reaction of aerobic ammonia oxidation to NH_2OH was −170.5 kJ

296 mol-NH_3^{-1} (**Supplementary text 1**), and this free energy (accounting for more than half of

297 $\Delta G_r'^o$ of aerobic ammonia oxidation) will be dissipated. Secondly, the oxidation of 1 mol

298 NH_2OH to NO_2^- releases 4 e^-, whereas the amounts of the e^- available for the respiration are

299 less than 2 e^- due to the following reasons; 1) the 2 e^- out of the produced 4 e^- is consumed to

300 oxidize 1 mol NH_3 to NH_2OH by Amo (Whittaker *et al.*, 2000), and 2) a part of the produced

301 4 e^- is consumed to generate NAD(P)H by reverse electron transport. In *Nitrosomonas*

302 *europaea* cells, the 0.35 e^- enters reverse electron flow (Whittaker *et al.*, 2000). Additionally,

303 the biochemistry of NH_2OH oxidation to NO_2^- by AOB is still controversial because the

304 *Nitrosomonas europaea* Hao oxidized NH_2OH to NO but not further to NO_2^-, and specific

305 mechanisms of NO oxidation to NO_2^- has not been elucidated (Carantoa and Lancaster, 2017;

306 Lancaster *et al.*, 2018). NO oxidation to NO_2^- releases 1 e^-, and the involvement of the

307 released e^- in the respiration of AOB needs to be investigated in other studies. The above

308 discussion pointed out that the amounts of the free energy recovered from aerobic ammonia

309 oxidation were much lower than that calculated as ΔG_r of the reaction. The reduction of the

310 free energy recovered from aerobic ammonia oxidation would result in the low free-energy

311 efficiencies of the ammonia oxidation reaction shown in **Table 2** (*i.e.*, 7 to 13%).

312 The ΔG_r of aerobic nitrite oxidation was much smaller than that of aerobic ammonia

313 oxidation (−83.5 kJ mol-NO_2^{-1} and −283.3 kJ mol-NH_3^{-1} at the batch incubation,

314 respectively,) (**Supplementary text 1**), while the CO_2 assimilation efficiency during aerobic

315 nitrite oxidation were close to that of the ammonia oxidation reaction; *i.e.*, 0.053 μmol-

316 CO_2/μmol-NO_2^- (**Table 2**). Such high CO_2 assimilation and free-energy efficiencies (31-32%)

317 were rarely observed from axenic cultures of NOB (*e.g.*, *Nitrospira marina* Nb-295; 0.032

318 μmol-CO_2/μmol-NO_2^- and 22%, respectively), but high biomass yield of marine NOB

319 (*Nitrospinae*) was previously found in environmental samples (Kitzinger *et al.*, 2020) where

320 the NOB coexisted with other microbes. Low free-energy efficiencies of aerobic nitrite

321 oxidation found in the axenic cultures were reasonable because NO_2^- oxidation reaction can

322 not couple with the reduction of quinone molecules (ubiquinone$_{ox/red}$, $\Delta E'^{o}$ = +0.11 V) directly

323 due to the high redox potential of NO_2^-/NO_3^- oxidation rection ($\Delta E'^{o}$ = +0.42 V) (Madigan *et*

324 *al.*, 2019). Additionally, the electrons released from the NO_2^- oxidation reaction enter to

325 terminal oxidase bypassing a cytochrome *bc1* complex (Lücker *et al.*, 2010; Simon and Klotz

326 *et al.*, 2013), resulting in the decrease of the number of translocated H^+ during the respiration:

327 therefore, the free-energy efficiencies of nitrite oxidation reaction were expected to be low.

328 On the other hand, *Nitrospira* in the NH_4^+- and NO_2^--feeding DHS reactors showed high CO_2

329 assimilation and free energy efficiencies. As compared with *Nitrobacter* and *Nitrococcus*, the

330 following bioenergetic advantages of the nitrite oxidation by *Nitrospira* were often introduced

331 in literatures; 1) nitrite oxidation occurs in the periplasmic spaces (Spieck *et al.*, 1998; Lücker

332 *et al.*, 2010), which directly contributes to the generation of proton motive force across a

333 membrane (*i.e.*, 1 NO_2^- + 1 H_2O → 1 NO_3^- + 2 $H^+_{periplasm}$ + 2 e^-), and 2) *Nitrospira* used an

334 energetically more efficient rTCA cycle for CO_2 fixation as compared with *Nitrobacter* and

335 *Nitrosococcus* who used the Calvin-Benson cycle. However, the difference of CO_2 fixation
336 pathway might not result in a drastic change of CO_2 assimilation efficiency although the
337 Calvin-Benson cycle requires more ATPs investment for CO_2 fixation and involves a wasteful
338 oxygenase side reaction of ribulose-1,5-bisphosphate carboxylase/oxygenase (Berg 2011;
339 Bayer *et al*., 2022). For the fixation of 3 mol CO_2 (*i.e*., HCO_3^-) to 1 mol of
340 phosphoglyceraldehyde which is the simplest sugar and a precursor for the biomass synthesis
341 (White *et al.*, 2012), the rTCA cycle requires 5 and 6 mol of ATP and NADPH equivalents
342 (such as NAD(P)H, ferredoxin and $FADH_2$), whereas the Calvin-Benson cycle requires 9 and
343 6 mol of ATP and NADPH equivalents (Bar-Even *et al.*, 2010). Therefore, the amounts of
344 NADPH equivalents are the same between the two pathways. To generate 6 mol of NAD(P)H
345 from $NAD(P)^+$ by the reverse electron transport, *Nitrosomonas europaea* and *Nitrobacter*
346 *winogradskyi* consumed 30 mol of ATP (Aleem, 1966; Sewell and Aleem, 1969); therefore,
347 the energy cost for reverse electron flow is >3 folds higher than that for CO_2 fixation. The
348 ATP cost of the rTCA cycle was 4 mol-ATP/mol-phosphoglyceraldehyde fewer than that of
349 the Calvin-Benson cycle, while this energy conservation is much smaller than the energy
350 consumption for reverse electron transport. Indeed, the CO_2 assimilation efficiencies
351 previously determined from marine *Nitrococcus* with Calvin-Benson cycle (*Nitrococcus*
352 *mobilis*) were comparable with that of marine *Nitrospira* with rTCA cycle (*Nitrospira marina*

353 Nb-295); *i.e.*, 0.014-0.031 and 0.032 μmol-CO_2/μmol-NO_2^-, respectively (Glover 1985; Bayer

354 *et al.*, 2022) (**Table 2**).

355 It is notable that NOB can receive some micronutrients produced in microbial

356 community (Mee *et al.*, 2014; Kim *et al.*, 2021), which would raise CO_2 assimilation

357 efficiencies of *Nitrospira*. One example is the vitamin-B_{12} auxotrophy of *Nitrospira marina*.

358 The *Nitrospira marina* genome lacked a couple of genes required for the biosynthesis of

359 vitamin B_{12}, and their growth ceased in vitamin-B_{12} deficient media (Bayer *et al.*, 2021).

360 However, the growth of *Nitrospira marina* was found in a mixed culture even when vitamin

361 B_{12} was not supplied into the media (Park *et al.*, 2020). Additionally, *Nitrospira* cells can

362 incorporate organic matters available in the culture. The addition of undefined organic matters

363 such as tryptone increased apparent growth yields of *Nitrospira marina* (Watson *et al.*, 1986;

364 Bayer *et al.*, 2021), and formate utilization by *Nitrospira* bacteria has been also demonstrated

365 (Gruber-Dorninger *et al.*, 2015; Koch *et al.*, 2015; Lawson *et al.*, 2021). Availability of

366 organic matters in the operated DHS reactors fed with inorganic media was suggested from

367 the growth of heterotrophic bacteria in the reactors. In the NH_4^+- and NO_2^--feeding DHS

368 reactors, heterotrophs (*i.e.*, the DHS20C01 to DHS20C21 bins) accounted for *ca*. 10% of total

369 biomass (**Table 1**), and the presence of those heterotrophs indirectly indicated that organic

370 matters were available in the operated DHS reactors (likely in the form of extracellular

371 polymeric substances, soluble microbial products and cell debris). The obtained *Nitrospira*

372 bins (and also NMNS bins, **Table S6**) had a couple of (di)peptide transporters and ABC
373 transporters, and scavenging micronutrients might contribute to the increase of apparent CO_2
374 assimilation efficiencies. In addition to the possible interactions of micronutrients, oxidative
375 stress in mixed communities would be less because coexisting microbes can scavenge O_2 and
376 reactive oxygen species. Less oxidative stress would reduce energy demands of the rTCA
377 cycle of *Nitrospira* where oxygen-sensitive enzymes (*e.g.*, four-subunit pyruvate:ferredoxin
378 oxidoreductase) are involved (Berg *et al.*, 2011; Bayer *et al.*, 2022).

379 Although the above discussion provided a bioenergetic insight in the CO_2
380 assimilation of AOB and NOB, the growth yields of AOB were still higher than those of NOB
381 including *Nitrospira* (**Table 2**). How did *Nitrospira* with lower CO_2 assimilation efficiencies
382 outnumbered *Nitrosomonas* in the NH_4^+-feeding DHS reactor? Notably, the DHS reactor and
383 the recirculating marine aquaculture systems in the previous studies were operated as trickling
384 filter reactors, and *Nitrospira* and AOB proliferated in the form of biofilm on the biomass
385 carriers (**Table S5**). The biomass carriers in those trickling filter reactors were exposed to
386 permanent shear forces, and shear forces changed microbial diversity and composition of the
387 developed biofilm (Rickard *et al.*, 2004) and promoted the proliferation of auto-aggregating
388 bacteria (Rochex *et al.*, 2008). In the nitrifying biofilm, AOB were preferentially localized on
389 the surface of the biofilm (*i.e.*, aerobic zone) whereas *Nitrospira* cells were easy to form cell
390 aggregates (Spieck *et al.*, 2006; Ushiki *et al.*, 2013) and heterologously distributed in the

391 biofilm and abundant in microaerobic zone (*i.e.*, inner part of biofilm) (Okabe *et al.*, 1999;

392 Schramm *et al.*, 2000). Such spatial distribution of AOB and NOB might occur in the sponge

393 carrier. Additionally, *Nitrospira* spp. in activated sludge tended to form physically stronger

394 cell aggregates than *Nitrosomonas oligotropha* (Larsen *et al*., 2008), suggesting

395 *Nitrosomonas* in the NH_4^+-feeding DHS reactor was likely to be more susceptible for the

396 detachment from biofilm. Occurrence of the washout of AOB and NOB from trickling filter

397 reactors has not been well investigated so far (Keuter *et al.*, 2011), which was examined in the

398 present study by determining the gene copy numbers of AOB *amoA*, *Nitrospira nxrB*, and

399 *Nitrospira* 16S rRNA genes (**Fig. 2**) in the NH_4^+-enriched biomass and the reactor effluents.

400 The NMNS01 bin had one copy of *amoCAB* gene cluster as well as the closed relative

401 *Nitrosomonas* genomes (*Nitrosomonas* sp. Nm143, *Nitrosomonas* sp. UBA8640, and

402 *Nitrosomonas aestuarii*). As for *Nitrospira*, three *nxrAB* gene clusters and one 16S rRNA

403 gene were found in the *Nitrospira marina* genome. This ratio of the copy number of *nxrAB* to

404 16S rRNA gene (*i.e.*, 3) agreed with the ratio of the copy numbers of *Nitrospira nxrB* to

405 *Nitrospira* 16S rRNA gene found in the NH_4^+-enriched biomass and the reactor effluents (*i.e.*,

406 3.0 to 3.4) (**Fig. 6**). Assuming one *amoA* gene copy per *Nitrosomonas* genome and three *nxrB*

407 and one 16S rRNA gene copy per *Nitrospira* genome, the abundance of *Nitrosomonas* was

408 1.5- and 1.7-folds greater (based on the normalized copy number of *nxrB* and 16S rRNA

409 gene, respectively) than *Nitrospira* in the effluents of NH_4^+-feeding DHS reactor although

410 *Nitrospira* was 1.89- and 1.86-folds greater than *Nitrosomonas* in NH_4^+-enriched biomass.

411 The greater abundance of *Nitrosomonas* in the effluents indicated that *Nitrosomonas* tended to

412 be washed out more frequently from the NH_4^+-feeding DHS reactor. This washout of AOB

413 was another determinant for the dominance of *Nitrospira* over *Nitrosomonas* in the NH_4^+-

414 feeding DHS reactors.

415 In summary, CO_2 assimilation efficiencies of *Nitrosomonas* and NO_2^--oxidizing

416 *Nitrospira* were determined, and the difference of the CO_2 assimilation efficiencies between

417 *Nitrosomonas* and *Nitrospira* was much smaller (0.077 μmol-CO_2/ μmol-NH_3 and 0.053−

418 0.054 μmol-CO_2/μmol-NO_2^-, respectively) as compared with the difference of ΔG_r. Such

419 small difference in the CO_2 assimilation efficiencies was likely due to that large parts of free

420 energies during aerobic ammonia oxidation are dissipated and not conserved. The dissipation

421 of free energy (*i.e.*, efficiency of energy conservation) can not be expected from the value of

422 ΔG_r, and more bioenergetic studies, especially for *Nitrospira*, are required. *Nitrospira* use a

423 novel cytochrome *bd*-like heme-copper oxidase as a terminal oxidase and the nitrite oxidation

424 occurs in periplasmic spaces, which were not common with that of canonical NO_2^--oxidizing

425 *Nitrobacter*. It will be interesting to investigate the bioenergetic traits of *Nitrospira*. Apart

426 from the bioenergetics, washout of nitrifying population was another factor driving the

427 dominance of *Nitrospira* over *Nitrosomonas* in the DHS reactor; *i.e.*, *Nitrosomonas* was more

428 susceptible for washout than *Nitrospira*. Detachment and washout of particular nitrifiers has

429 been little explored, and the correlation between physicochemical parameters (*e.g.*, cell

430 surface hydrophobicity) remains to be explored in other studies.

431 **Experimental procedures**

432 ***Operation of the DHS reactors fed with NH_4^+ or NO_2^-***

433 The 10-L DHS reactors (0.7 m in height and 0.17 m in width) were operated at 20ºC in dark.

434 Details of the operated DHS reactors were previously described by the authors (Oshiki *et al.,*

435 2020). Briefly, the DHS reactors contained polyurethane-sponge media (183 pieces of cubic

436 sponge, 33 mm × 33 mm × 33 mm, set in a polypropylene tube, 32 mm diameter and 32 mm

437 long) as a biomass carrier. The sponge media had a 97% void ratio (*i.e.*, a percentage of the

438 volume of sponge pores), 256 m^2 m^{-3} of specific surface, and 0.63 mm of average pore size.

439 Artificial seawater media (pH 8.0, salinity 33‰) containing 0.297 g L^{-1} NH_4Cl or 0.4 g L^{-1}

440 $NaNO_2^-$, 1 g L^{-1} $NaHCO_3$, 34 g L^{-1} artificial seawater powder (Marin Art, Tomita

441 Pharmaceutical, Naruto, Japan) was supplied to the top of the DHS reactor at the flow rate of

442 9.62 L d^{-1} corresponding to 0.39 d of hydraulic retention time (HRT) and 200 mg-N L-sponge

443 $media^{-1}$ d^{-1} of total ammonia nitrogen loading rate. The sponge media was exposed to the

444 atmosphere, and oxygen naturally dissolved into the media and aerobic condition was

445 maintained without external aeration. The filtrates were collected in a settling tank (volume;

446 0.9 L) located at the bottom of the DHS reactor, which were recirculated using a magnetic

447 pump at the flow rate of 4 L min^{-1}. The NH_4^+- or NO_2^--feeding DHS reactors has been

448 operated for more than 1 y stably, and typical concentrations of NH_4^+, NO_2^-, NO_3^- and pH

449 values in the NH_4^+-feeding DHS reactors were 7.9 μM, 9.3 μM, 4.9 mM, and pH 7.3,

450 respectively.

451 Biomass retained in the sponge media was collected by squeezing the sponge media

452 in the above artificial seawater media without NH_4Cl and $NaNO_2^-$, and subjected to the

453 following DNA extraction and batch incubations. As for the reactor effluents, two liters of the

454 effluents was daily collected from the NH_4^+-feeding reactor for 4 d, and the collected

455 effluents were filtered on a 0.2 μm-pore-size PVDF membrane (Advantec, Tokyo, Japan)

456 separately. The filtered membranes were subjected to the DNA extraction.

457 ***DNA extraction and determination of DNA concentration***

458 Genomic DNA was extracted from the biomass and the filtered membranes using a DNeasy

459 PowerSoil kit (Qiagen K.K., Tokyo, Japan) as following the instruction manual supplied by

460 manufactures. The concentrations of the extracted DNAs were determined using the Qubit

461 dsDNA BR assay kit and a Qubit 3.0 fluorospectrometer (Thermo Fisher Scientific, Waltham,

462 MD, USA).

463 ***Metagenomic analysis***

464 A shotgun sequence library was prepared using a MGIEasy FS DNA Library Prep Set,

465 MGIEasy Circularization kit, and DNBSEQ-G400RS High-throughput sequencing set (MGI

466 Tech Japan, Tokyo, Japan). The 200-bp paired-end sequencing was performed using a

467 DNBSEQ-G400 sequencer. The paired-end sequence reads were trimmed using Trimmomatic

468 0.39 (SLIDINGWINDOW:6:30 MINLEN:100) (Bolger *et al.*, 2014). Digital normalization of
469 trimmed sequences was performed using bbnorm.sh of BBtools version 38.18 (target=100,
470 min=5) (https://jgi.doe.gov/data-and-tools/bbtools/). Assembled contigs were obtained from
471 NH_4^+- and NO_2^--enriched biomass samples (co-assembly) by Megahit v1.2.9 (--k-min 27 --k-
472 max 141 --k-step 12) (Li *et al.*, 2015). Reads of each sample were mapped to assembled
473 contigs using bbmap.sh of BBtools. Obtained contigs of short length (< 2,500 bp) were
474 removed before binning. The multiple software of MaxBin2 version 2.15 (-markerset 40) (Wu
475 *et al*., 2016), Metabat2 version 2.2.7 (Kang *et al.*, 2019), MyCC (MyCC_2017.ova) (Lin and
476 Liao, 2016) were used for binning from the contigs. To refine the obtained bins, we used
477 Binning_refiner version 1.4.0 with default parameters (Song and Thomas, 2017). The quality
478 of refined bins was checked using CheckM version 1.0.7 (Parks *et al.*, 2014). The relative
479 abundance of obtained bins was calculated using CoverM version 0.6.1
480 (https://github.com/wwood/CoverM#installation). Phylogenetic position of each bin is
481 estimated using GTDBtk v1.3.0 (release95) (Chaumeil *et al.*, 2019). Average nucleotide
482 identity (ANI) values of the obtained *Nitrospira* bins and the genomes in *Nitrospira*
483 sublineage IV were calculated using pyani version 0.2.11 (-m ANIb) (Pritchard *et al*., 2016).
484 Gene prediction and annotation was performed via the D-FAST pipeline (Tanizawa *et al.*,
485 2018), and the MetaGeneAnnotator and Glimmer version 2.10, tRNAScan-SE version 1.23,

486 and blastn software applications were used for prediction of gene-coding sequences (CDSs),
487 tRNA, and rRNA, respectively.
488 Genomic tree was constructed using 120 concatenated phylogenetic marker genes of
489 obtained bins and representatives of genus *Nitrospira* or *Nitrosomonas* in the release95 of
490 GTDBtk version 1.3.0. For the multiple sequence alignment of *Nitrospira* spp., we included
491 the genomes of *Nitrospira marina* Nb-295T, *Nitrospirales* bacterium isolate MH-Pat-
492 all_autometa_1-10 (WLXC01000001), MAG-Baikal-G1, MAG-Baikal-deep-G158, MAG-
493 Baikal-deep-G159, MAG-ZH-13may13-77, MAG-cas150m-170, MAG-cas50m-175 with
494 *Nitrospira* genomes in the release95 of GTDBtk. Conserved marker genes were identified
495 using "gtdbtk identify" with default parameters and aligned to reference genomes using
496 "gtdbtk align" with taxonomic filters for phylogenies of *Nitrospira* (--taxa_fileter
497 c__Nitrospira), Nitrosomonas (--taxa_fileter f_Nitrosomonadaceae) or all metagenomic bins
498 (--taxa_fileter
499 f__UBA8639,g__Nitrosomonas,f__UBA11606,o__ARS69,f__Saprospiraceae,g__SZUA-
500 3,g__GCA-2699125,g__CR02bin9,f__Nitrospinaceae,f__SM1A02,g__UBA1845,f__B15-
501 G4,g__Hyphobacterium,g__Marinicaulis,g__UBA5701,g__Minwuia,f__Methyloligellaceae,f
502 __Rhodomicrobiaceae,g__UBA9145,o__UBA10353,g__UBA7359,o__Xanthomonadales).
503 Phylogenetic tree was constructed using IQ-TREE version 2.0.3 (-B 1000) with automatically
504 optimized substitution models (*Nitrospira*: LG+F+R7 and *Nitrosomonas*: JTT+F+R5) (Minh

505 *et al.*, 2020) and with the *Nitrosospira lacus* (GCF_000355765.4) and *Thermodesulfovibrio*

506 *yellowstonii* (GCF_000020985.1) genomes for the *Nitrospira* and *Nitrosomonas* trees (**Fig. 2**

507 and **3**, respectively) as an outgroup.

508 ***qPCR assay***

509 The qPCR assay was conducted using a ABI7500 fast Real-Time PCR System (Thermo

510 Fisher Scientific). The reaction mixture (10 μL) contained KAPA SYBR FAST qPCR master

511 mix (Nippon Genetics, Tokyo, Japan) (5 μL), 0.2 μM each forward and reverse primer, 1 ×

512 ROX low dye, and 1 ng of the extracted DNA. Oligonucleotide primers used for PCR

513 amplification were 1) 515f and 806r for prokaryotic 16S rRNA gene, 2) amoA1F and

514 amoA2Rv1 for AOB *amoA* (Rotthauwe *et al.,* 1997, this study), 3) nxrB169f and nxrB638r

515 (Pester *et al.,* 2014) for *Nitrospira nxrB*, and 4) Nspra675F and Nspra746R (Graham *et al.,*

516 2007) for *Nitrospira* 16S rRNA gene, and the nucleotide sequences were shown in **Table S6**.

517 The original amoA2R primer (Rotthauwe *et al.,* 1997) had some mismatch bases against the

518 *amoA* sequence found in the NMNS01 bin, and the amoA2Rv1 was designed in the present

519 study by adding degenerate bases into the amoA2R primer. As for the amoA1F, nxrB169f,

520 nxrB638r, Nspra675F, and Nspra746R primers, there was no mismatch base between the

521 oligonucleotide primer and target gene found in the above metagenomic analysis. The cycling

522 conditions were the following: 95°C for 3 min; 40 cycles at 95°C for 3 s and 60°C for 20 s;

523 and, finally, 65°C to 95°C in 0.5°C increments for the melting curve analysis. Standard curves

524 (10^1 to 10^6 copies/μL) were prepared using a dilution series of plasmid DNAs containing PCR

525 products of the above target. Partial sequences of *Escherichia coli* JM109 (SMOBIO

526 technology, Hsinchu, Taiwan) 16S rRNA gene, *Nitrosomonas europaea* (NBRC14298)

527 *amoA*, *Nitrospira inopinata* (JCM31988) 16S rRNA gene were amplified using the above

528 oligonucleotide primer set. *Nitrospira nxrB* was amplified using the genomic DNA extracted

529 from NO_2^--enriched biomass. The obtained PCR products were cloned into pUC118 vector

530 using mighty cloning reagent (TakaraBio, Shiga, Japan), and transformed into *E. coli* DH5α

531 cells (SMBIO technology) by heat shock. Plasmids were extracted from the transformants

532 using FastGene Plasmid mini kit (Nippon Genetics), nucleotide sequences of the cloned PCR

533 products were ascertained by performing the Sanger sequencing, and the concentrations of the

534 extracted plasmids were determined fluorometrically as previously described above.

535 ***Activity tests***

536 Assimilation of $^{14}CO_2$ into the biomass during aerobic ammonia and nitrite oxidation

537 was examined as previously described (Oshiki *et al.,* 2011). Briefly, the 2.5 mL of biomass

538 suspension (24 and 0.66 μg-protein mL^{-1} of biomass concentrations for NH_4^+- and NO_2^--

539 enriched biomass, respectively) containing 0.5 mM NH_4^+ or NO_2^- was incubated at 20ºC in

540 10-mL glass vials with shaking at 60 rpm. The ^{14}C-labeled sodium bicarbonate (Moravek Inc.,

541 Brea, CA, USA) was added at a concentration of 10 μCi $vial^{-1}$, and the vials were sealed with

542 butyl rubber plug and aluminum seal. After 18 h of incubation, the biomass was fixed with

543 4% paraformaldehyde, washed three times with PBS, and mixed with scintillation cocktail

544 Clear-sol I (Nacalai, Tokyo, Japan). Radioactivity was determined with an ALOKA LSC-

545 6100 liquid scintillation counter. Additional cold incubation with ^{12}C-labeled sodium

546 bicarbonate instead of ^{14}C-labeled one was performed in parallel to determine ammonia and

547 nitrite oxidation rates. Abiotic incorporation of ^{14}C-labeled sodium bicarbonate was examined

548 by performing the above incubation with the biomass pasteurized at 70ºC for 15 min. For the

549 incubation using H_2 as a substrate instead of NH_4^+ and NO_2^-, biomass suspension without

550 NH_4^+ and NO_2^- were dispensed into the closed vials, and pure H_2 gas (GL Science, Tokyo,

551 Japan) was injected into headspace at the final concentration of 2% (v/v) using a gas tight

552 syringe.

553 ***<u>Chemical analysis</u>***

554 NH_4^+ concentration was determined fluorometrically using the *o*-phthalaldehyde (OPA)

555 method (Taylor *et al.,* 1974). Liquid samples were mixed with 3.8 mM *o*-phthalaldehyde, and

556 fluorescence intensity was determined at 355 nm of excitation and 460 nm of emission.

557 NO_2^- concentration was determined colorimetrically using the

558 naphthylethylenediamine method (Rice *et al.,* 2012). Liquid samples were mixed with a

559 naphthylethylenediamine-sulfanilamide solution, and absorbance was measured at 540 nm.

560 NO_3^- concentration was determined colorimetrically using the brucine sulfate

561 method (Jenkins and Medsker*,* 1964). Liquid samples were mixed with 80% (vol/vol) sulfuric

562 acid and brucine sulfanilic acid solution, and heated at 100ºC for 20 min. The absorbance was

563 measured at 410 nm.

564 Protein concentration was determined by the Lowry method using a DC protein

565 assay kit (Bio-Rad, Hercules, CA, USA). Bovine serum albumin was used as a protein

566 standard.

567 H_2 concentration was determined by gas chromatography as described elsewhere.

568 The 100 µL of gas sample was injected into a gas chromatograph GC-2014 equipped with a

569 thermal conductivity detector and a 2-m stainless column packed with a Molecular Sieve-5A.

570 ***Fluorescence in-situ hybridization and microscopy***

571 Fixation of biomass (4% paraformaldehyde) and *in situ* hybridization of oligonucleotide

572 probes were performed as previously described (Kindaichi *et al.,* 2004). The fixed biomass

573 was sonicated at 3 watt for 4 minutes, and hybridized with the oligonucleotide probe

574 Ntspa712 (Daims *et al*., 2001) for *Nitrospira* or Nsm156 (Mobarry *et al*., 1996) for

575 *Nitrosomonas*, respectively.

576 ***Calculation of CO_2 assimilation and free-energy efficiencies.***

577 CO_2 assimilation efficiencies of NH_4^+- and NO_2^--enriched biomass during aerobic ammonia

578 and nitrite oxidation (unit; µmol-CO_2/µmol-NH_3 or µmol-NO_2^-) were calculated by dividing

579 the molar amounts of $^{14}CO_2$ fixed during the incubation with those of the consumed NH_4^+ and

580 NO_2^-. The fixed CO_2 includes the carbon fixed into cellular materials and also that fixed as

581 extracellular polymeric substances (EPS) (Okabe *et al*., 2005). On the other hand, the fixed

582 CO_2 does not include the carbon released as dissolved organic carbon (DOC); *i.e.*, *ca*. 6-8%

583 and 12% of fixed CO_2 were released as DOC in the culture of marine AOB (*Nitrosomonas*

584 *marina* C-25 and *Nitrosomonas* sp. C-15) and marine NOB (*Nitrospira marina* Nb-295),

585 respectively (Bayer *et al*., 2022).

586 The values of free-energy efficiency were calculated using the following equation

587 (Glover, 1985).

588 $$free - energy\ efficiency\ (\%) = growth\ yield\ \times \frac{495}{\Delta G_r} \times 100$$

589 Where, 495; the free energy (kJ/mol) required for converting CO_2 into CH_2O, and ΔG_r; the

590 free energy (kJ/mol) obtained from aerobic ammonia or nitrite oxidation during the batch

591 incubations (*i.e*., 283.3 kJ /mol-NH_3 and 83.5 kJ /mol-NO_2^-, respectively) (**Supplementary**

592 **text 1**). For AOB and NOB examined in the previous studies, the 286.7 kJ /mol-NH_3 for

593 AOB, and 73.8 kJ /mol-NO_2^- for NOB were used. Those values corresponded to $\Delta G_r'^m$ that

594 were the Gibbs free energy change at when the concentrations of all reactants were 1 mM at

595 pH 7 and 25ºC (**Supplementary text 1**).

596 ***<u>Accession numbers</u>***

Raw metagenomic sequence data and the assembled and annotated 30 bins obtained in the present study are available in the DDBJ nucleotide sequence database under the accession number DRA013035 and those in **Table S7**, respectively.

Acknowledgements

This work was supported by JSPS KAKENHI [grant numbers; 19K05805 for M.O., 20H02290 for N.A, 20H00641 for T.Y., 19H00776 for S.O.], JST FOREST Program [JPMJFR216Z for M.O.], and Nagase Science and Technology Foundation granted to M.O.. Computations were partially performed on the NIG supercomputer at ROIS National Institute of Genetics. The authors would like to express our sincere appreciation for Dr. Barbara Bayer (University of Vienna) for sharing a reference dataset of the DIC fixation yields of nitrifiers that are shown in **Table 2**. Strain JCM31988 and NBRC14298 were provided by Japan Collection of Microorganisms, RIKEN BRC and National Institute of Technology and Evaluation, respectively.

Conflict of interest

The authors declare no conflicts of interest associated with this manuscript.

612 **References**

613 Aleem, M.I.H. (1966) Generation of reducing power in chemosynthesis. II. Energy-linked
614 reduction of pyridine nucleotides in the chemoautotroph, *Nitrosomonas europaea*.
615 *Biochim Biophys Acta* **113**: 216–224.

616 Ali, M., Oshiki, M., Awata, T., Isobe, K., Kimura, Z., Yoshikawa, H., Hira, D., Kindaichi, T.,
617 Satoh, H., Fujii, T., Okabe, S., (2015) Physiological characterization of anaerobic
618 ammonium oxidizing bacterium "*Candidatus* Jettenia caeni." *Environ. Microbiol.* **17**:
619 2172–2189.

620 Awata, T., Kindaichi, T., Ozaki, N., Ohashi, A., 2015. Biomass yield efficiency of the marine
621 anammox bacterium, "*Candidatus* Scalindua sp.," is affected by salinity. *Microb.*
622 *Environ*. **30**: 86–91.

623 Bar-Even, A., Noor, E., Lewis N.E., and Milo, R. (2010) Design and analysis of synthetic
624 carbon fixation pathways. *Proc Natl Acad Sci USA* **107**: 8889–8894.

625 Bayer, B., Saito, M.A., McIlvin, M.R., Lücker, S., Moran, D.M., Lankiewicz, T.S., et al.
626 (2021) Metabolic versatility of the nitrite-oxidizing bacterium *Nitrospira marina* and
627 its proteomic response to oxygen-limited conditions. *ISME J* **15**: 1025-1039.

628 Bayer, B., McBeain, K., Carlson, C.A., Santoro, A.E. (2022) Carbon content, carbon fixation
629 yield and dissolved organic carbon release from diverse marine nitrifiers. *bioRxiv*
630 2022.01.04.474793. https://doi.org/10.1101/2022.01.04.474793

631 Berg, I.A. (2011) Ecological aspects of the distribution of different autotrophic CO_2 fixation
632 pathways. *Appl Environ Microbiol* **77**: 1925–1936.
633 Bergmann, D.J., Hooper, A.B., Klotz, M.G. (2005) Structure and sequence conservation of
634 hao cluster genes of autotrophic ammonia-oxidizing bacteria: evidence for their
635 evolutionary history. *Appl. Environ. Microbiol.* **71**: 5371–5382.
636 Bock, E., Schmidt, I., Stüven, R., Zart, D., (1995) Nitrogen loss caused by denitrifying
637 *Nitrosomonas* cells using ammonium or hydrogen as electron donors and nitrite as
638 electron acceptor. *Arch. Microbiol.* **163**: 16–20.
639 Bolger, A.M., Lohse, M., and Usadel, B. (2014) Trimmomatic: a flexible trimmer for Illumina
640 sequence data. *Bioinformatics* **30**: 2114–2120.
641 Brown, M.N., Briones, A., Diana, J., and Raskin, L. (2013) Ammonia-oxidizing archaea and
642 nitrite-oxidizing *nitrospiras* in the biofilter of a shrimp recirculating aquaculture
643 system. *FEMS Microbiol Ecol* **83**: 17–25.
644 Carantoa, J.D., and Lancaster, K.M. (2017) Nitric oxide is an obligate bacterial nitrification
645 intermediate produced by hydroxylamine oxidoreductase. *Proc Natl Acad Sci U S A*
646 **114**: 8217–8222.
647 Chaumeil, P.A., Mussig, A.J., Hugenholtz, P., and Parks, D.H. (2019) GTDB-Tk: a toolkit to
648 classify genomes with the Genome Taxonomy Database. *Bioinformatics* **36**: 1925–
649 1927.

650 Costa, E., Pérez, J., and Kreft, J-U. (2006) Why is metabolic labour divided in nitrification?
651 *Trends Microbiol* **14**: 213–219.
652 Daebeler, A., Kitzinger, K., Koch, H., Herbold, C.W., Steinfeder, M., Schwarz, J., et al.
653 (2020) Exploring the upper pH limits of nitrite oxidation: diversity, ecophysiology,
654 and adaptive traits of haloalkalitolerant *Nitrospira*. *ISME J* **14**: 2967–2979.
655 Daims, H., Nielsen, J.L., Nielsen, P.H., Schleifer, K.-H., Wagner, M. (2001) In situ
656 characterization of *Nitrospira*-like nitrite-oxidizing bacteria active in wastewater
657 treatment plants. *Appl. Environ. Microbiol.* **67**: 5273–5284.
658 Daims, H., Lebedeva, E.V., Pjevac, P., Han, P., Herbold, C., Albertsen, M., et al. (2015)
659 Complete nitrification by *Nitrospira* bacteria. *Nature* **528**: 504–509.
660 Daims, H., Lücker, S., and Wagner, M. (2016) A new perspective on microbes formerly
661 known as nitrite-oxidizing bacteria. *Trends Microbiol* **24**: 699–712.
662 Foesel, B.U., Gieseke, A., Schwermer, C., Stief, P., Koch, L., Cytryn, E., et al. (2008)
663 *Nitrosomonas* Nm143-like ammonia oxidizers and *Nitrospira marina*-like nitrite
664 oxidizers dominate the nitrifier community in a marine aquaculture biofilm. *FEMS*
665 *Microbiol Ecol* **63**: 192–204.
666 Graham, D.W., Knapp C.W., Van Vleck, E.S., Bloor, K., Lane, T.B., and Graham, C.E.
667 (2007) Experimental demonstration of chaotic instability in biological nitrification.
668 *ISME J* **1**: 385–393.

669 Glover, H.E. (1985) The relationship between inorganic nitrogen oxidation and organic
670 carbon production in batch and chemostat cultures of marine nitrifying bacteria. *Arch*
671 *Microbiol* **142**: 45–50.
672 Gruber-Dorninger, C., Pester, M., Kitzinger, K., Savio, D.F., Loy, A., Rattei, T., et al. (2015)
673 Functionally relevant diversity of closely related *Nitrospira* in activated sludge. *ISME*
674 *J* **9**: 643–655.
675 Hollocher, T.C., Kumar, S., and Nicholas, D.J. (1982) Respiration-dependent proton
676 translocation in *Nitrosomonas europaea* and its apparent absence in *Nitrobacter agilis*
677 during inorganic oxidations. *J Bacteriol* **149**: 1013–1020.
678 Itoi, S., Niki, A., and Sugita, H. (2006) Changes in microbial communities associated with the
679 conditioning of filter material in recirculating aquaculture systems of the pufferfish
680 *Takifugu rubripes*. *Aquaculture* **256**: 287–295.
681 Jenkins, D., and Medsker, L.L. (1964) Brucine method for determination of nitrate in ocean,
682 estuarine, and fresh waters. *Anal Chem* **36**: 610–612.
683 Kang, D.D., Li, F., Kirton, E., Thomas, A., Egan, R., An, H., and Wang, Z. (2019) MetaBAT
684 2: an adaptive binning algorithm for robust and efficient genome reconstruction from
685 metagenome assemblies. PeerJ. **7**: e7359.

686 Keuter, S., Kruse, M., Lipski, A., and Spieck, E. (2011) Relevance of *Nitrospira* for nitrite
687 oxidation in a marine recirculation aquaculture system and physiological features of a
688 *Nitrospira marina*-like isolate. *Environ Microbiol* **13**: 2536–2547.
689 Keuter, S., Beth, S., Quantz, G., Schulz, C., and Spieck, E. (2017) Longterm monitoring of
690 nitrification and nitrifying communities during biofilter activation of two marine
691 recirculation aquaculture systems (RAS). *Int J Aquacult Fish Sci* **3**: 051–061.
692 Kim, S., Kang, I., Lee, J-W., Jeon, C.O., Giovannoni, S.J., and Cho, J-C. (2021) Heme
693 auxotrophy in abundant aquatic microbial lineages. *Proc. Natl. Acad. Sci. U. S. A.* **118**:
694 e2102750118.
695 Kindaichi, T., Ito, T., and Okabe, S. (2004) Ecophysiological interaction between nitrifying
696 bacteria and heterotrophic bacteria in autotrophic nitrifying biofilms as determined by
697 microautoradiography-fluorescence *in situ* hybridization. *Appl Environ Microbiol* **70**:
698 1641–1650.
699 Kitzinger, K., Marchant, H.K., Bristow, L.A., Herbold, C.W., Padilla, C.C., Kidane, A.T., et
700 al. (2020) Single cell analyses reveal contrasting life strategies of the two main
701 nitrifiers in the ocean. *Nat Commun* **11**: 767.
702 Koch, H., Galushko, A., Albertsen, M., Schintlmeister, A., Gruber-Dorninger, C., Lücker, S.,
703 et al. (2014) Growth of nitrite-oxidizing bacteria by aerobic hydrogen oxidation.
704 *Science* **345**: 1052–1054.

Koch, H., Lücker, S., Albertsen, M., Kitzinger, K., Herbold, C., Spieck, E., et al. (2015) Expanded metabolic versatility of ubiquitous nitrite-oxidizing bacteria from the genus *Nitrospira*. *Proc Natl Acad Sci U S A* **112**: 11371–11376.

Lancaster, K.M., Caranto, J.D., Majer, S.H., and Smith, M.A. (2018) Alternative bioenergy: updates to and challenges in nitrification metalloenzymology. *Joule* **2**: 421–441.

Larsen, P., Nielsen, J.L., Svendsen, T.C., Nielsen, P.H. (2008) Adhesion characteristics of nitrifying bacteria in activated sludge. *Water Res.* **42**: 2814–2826.

Lawson, C.E., Mundinger, A.B., Koch, H., Jacobson, T.B., Weathersby, C.A., Jetten, M.S.M., et al. (2021) Investigating the chemolithoautotrophic and formate metabolism of *Nitrospira moscoviensis* by constraint-based metabolic modeling and ^{13}C-tracer analysis. mSystems ; 6: e00173-21.

Lebedeva, E.V., Off, S., Zumbrägel, S., Kruse, M., Shagzhina, A., Lücker, S., et al. (2011) Isolation and characterization of a moderately thermophilic nitrite-oxidizing bacterium from a geothermal spring: Moderately thermophilic *Nitrospira*-cultures from hot springs. *FEMS Microbiol. Ecol.* **75**: 195–204.

Li, D., Liu, CM., Luo, R., Sadakane, K., and Lam, TW. (2015) MEGAHIT: an ultra-fast single-node solution for large and complex metagenomics assembly via succinct de Bruijn graph. *Bioinformatics* **31**: 1674–1676.

723 Lin, H.H., and Liao, Y.C. (2016) Accurate binning of metagenomic contigs via automated
724 clustering sequences using information of genomic signatures and marker genes. *Sci*
725 *Rep* **6:** 24175.
726 Lücker, S., Wagner, M., Maixner, F., Pelletier, E., Koch, H., Vacherie, B., et al. (2010) A
727 *Nitrospira* metagenome illuminates the physiology and evolution of globally
728 important nitrite-oxidizing bacteria. *Proc Natl Acad Sci U S A* 107: 13479–13484.
729 Madigan, M.T., Bender, K.S., Buckley, D.H., Sattley, W.M., and Stahl, D.A. (eds). (2019)
730 *Brock biology of microorganisms*, 15th. edn. New York, USA: Pearson Education.
731 Mee, M.T., Collins, J.J., Church, G.M., and Wang, H.H. (2014) Syntrophic exchange in
732 synthetic microbial communities. *Proc. Natl. Acad. Sci. U. S. A.* 111: E2149–E2156.
733 Minh, B.Q., Schmidt, H.A., Chernomor, O., Schrempf, D., Woodhams, M.D., von Haeseler,
734 A., et al. (2020) IQ-TREE 2: new models and efficient methods for phylogenetic
735 inference in the genomic era. *Mol. Biol. Evol.* **37**: 1530–1534.
736 Mobarry, B.K., Wagner, M., Urbain, V., Rittmann, B.E., and Stahl, D.A. (1996) Phylogenetic
737 probes for analyzing abundance and spatial organization of nitrifying bacteria. *Appl.*
738 *Environ. Microbiol.* **62**: 2156-2162.
739 Okabe, S., Satoh, H., and Watanabe, Y. (1999) In situ analysis of nitrifying biofilms as
740 determined by in situ hybridization and the use of microelectrodes. *Appl Environ*
741 *Microbiol* **65**: 3182–3191.

742 Okabe, S., Kindaichi, T., Ito, T. (2005). Fate of ^{14}C-labeled microbial products derived from
743 nitrifying bacteria in autotrophic nitrifying biofilms. *Appl Environ Microbiol* **71**:
744 3987–3994.
745 Oshiki, M., Shimokawa, M., Fujii, N., Satoh, H., and Okabe, S. (2011) Physiological
746 characteristics of the anaerobic ammonium-oxidizing bacterium '*Candidatus* Brocadia
747 sinica'. *Microbiology* **157**: 1706–1713.
748 Oshiki, M., Aizuka, T., Netsu, H., Oomori, S., Nagano, A., Yamaguchi, T., et al. (2020) Total
749 ammonia nitrogen (TAN) removal performance of a recirculating down-hanging
750 sponge (DHS) reactor operated at 10 to 20ºC with activated carbon. *Aquaculture* **520**:
751 734963.
752 Parks, D.H., Imelfort, M., Skennerton, C.T., Hugenholtz, P., and Tyson, G.W. (2014)
753 Assessing the quality of microbial genomes recovered from isolates, single cells, and
754 metagenomes. *Genome Res* **25**: 1043-1055.
755 Park, S-J., Andrei, A-Ş., Bulzu, P-A., Kavagutti, V.S., Ghai, R., and Mosier, A.C. (2020)
756 Expanded diversity and metabolic versatility of marine nitrite-oxidizing bacteria
757 revealed by cultivation- and genomics-based approaches. *Appl Environ Microbiol* **86**:
758 e01667-20.

759 Pester, M., Maixner, F., Berry, D., Rattei, T., Koch, H., Lücker, S., et al. (2014) NxrB
760 encoding the beta subunit of nitrite oxidoreductase as functional and phylogenetic
761 marker for nitrite-oxidizing *Nitrospira*. *Environ Microbiol* **16**: 3055–3071.
762 Pritchard, L., Glover, R.H., Humphris, S., Elphinstone, J.G., Toth, I.K. (2016) Genomics and
763 taxonomy in diagnostics for food security: soft-rotting enterobacterial plant pathogens.
764 *Anal. Methods* **8**: 12–24.
765 Rice, E.W., Baird, R.B., Eaton, A.D., and Clesceri, (eds). (2012) *Standard methods for the*
766 *examination of water and wastewater*, 22th edn. Washington, USA: American public
767 health association.
768 Richter, M., and Rosselló-Móra, R. (2006) Shifting the genomic gold standard for the
769 prokaryotic species definition. *Proc Natl Acad Sci U S A* **106**: 19126–19131.
770 Rickard, A.H., McBain, A.J., Stead, A.T., and Gilbert, P. (2004) Shear rate moderates
771 community diversity in freshwater biofilms. *Appl Environ Microbiol* **70**: 7426–7435.
772 Rochex, A., Godon, J-J., Bernet, N., and Escudié, R. (2008) Role of shear stress on
773 composition, diversity and dynamics of biofilm bacterial communities. *Water Res* **42**:
774 4915–4922.
775 Rotthauwe, J-H., Witzel, K-P., and Liesack, A.W. (1997) The ammonia monooxygenase
776 structural gene *amoA* as a functional marker: molecular fine-scale analysis of natural
777 ammonia-oxidizing populations. *Appl Environ Microbiol* **63**: 4704–4712.

Schramm, A., Beer, D.D., Gieseke, A., and Amann, R. (2000) Microenvironments and distribution of nitrifying bacteria in a membrane-bound biofilm. *Environ Microbiol* **2**: 680–686.

Sedlacek, C.J., McGowan, B., Suwa, Y., Sayavedra-Soto, L., Laanbroek, H.J., Stein, L.Y., et al. (2019) A physiological and genomic comparison of *Nitrosomonas* cluster 6a and 7 ammonia-oxidizing bacteria. *Microbial Ecol* **78**: 985–994.

Sewell, D.L., and Aleem, M.I.H. (1969) Generation of reducing power in chemosynthesis. V. The mechanism of pyridine nucleotide reduction by nitrite in the chemoautotroph *Nitrobacter agilis*. *Biochim Biophys Acta* **172**: 467–475.

Simon, J., and Klotz, M.G. (2013) Diversity and evolution of bioenergetic systems involved in microbial nitrogen compound transformations. Biochim Biophys Acta **1827**: 114–135.

Song, W.Z., and Thomas, T. (2017) Binning_refiner: Improving genome bins through the combination of different binning programs. *Bioinformatics* **33**: 1873-1875.

Spieck, E., Ehrich, S., Aamand, J., and Bock, E. (1998) Isolation and immunocytochemical location of the nitrite-oxidizing system in *Nitrospira moscoviensis*. *Arch Microbiol* **169**: 225–230.

795 Spieck, E., Hartwig, C., McCormack, I., Maixner, F., Wagner, M., Lipski, A., et al. (2006)
796 Selective enrichment and molecular characterization of a previously uncultured
797 *Nitrospira*-like bacterium from activated sludge. *Environ Microbiol* **8**: 405–415.
798 Tanizawa, Y., Fujisawa, T., and Nakamura, Y. (2018) DFAST: a flexible prokaryotic genome
799 annotation pipeline for faster genome publication. *Bioinformatics* **34**: 1037–1039.
800 Taylor, S., Ninjoor, V., Dowd, D.M., and Tappel, A.L. (1986) Cathepsin B_2 measurement by
801 sensitive fluorometric ammonia analysis. *Anal Chem* 1974; **60**: 153–162.
802 Tsai Y.L., and Tuovinen O.H. Molar growth yield of *Nitrobacter agilis* in batch culture. *Can*
803 *J Microbiol* **32**: 605–606.
804 Ushiki, N., Fujitani, H., Aoi, Y., and Tsuneda, S. (2013) Isolation of *Nitrospira* belonging to
805 sublineage II from a wastewater treatment plant. *Microbes Environ* **28**: 346–353.00.
806 VanBriesen, J.M. (2001) Thermodynamic yield predictions for biodegradation through
807 oxygenase activation reactions. *Biodegradation* **12**: 265–281.
808 van Kessel, M.A.H.J. van Speth, D.R., Albertsen, M., Nielsen, P.H., Camp, H.J.M.O. den,
809 Kartal, B., et al. (2015) Complete nitrification by a single microorganism. *Nature* **528**:
810 555–559.
811 Watson, S.W., Book, E., Valois, F.W., Waterbury, J.B., Schlosser, U. (1986) *Nitrospira*
812 *marina* gen. nov. sp. nov.: a chemolithotrophic nitrite-oxidizing bacterium. *Arch*
813 *Microbiol* **144**: 1–7.

814 White, D., Drummond, J., and Fuqua, C. (eds). (2012) *The physiology and biochemistry of*
815 *prokaryotes*, 4th edn. New York, USA: Oxford University Press.
816 Whittaker, M., Bergmann, D., Arciero, D., and Hooper, A.B. (2000) Electron transfer during
817 the oxidation of ammonia by the chemolithotrophic bacterium *Nitrosomonas*
818 *europaea*. *Biochim Biophys Acta* **1459**: 346–355.
819 Wu, Y.W., Simmons, B.A., and Singer, S.W. (2016) MaxBin 2.0: an automated binning
820 algorithm to recover genomes from multiple metagenomic datasets. *Bioinformatics* **32**:
821 605–607.
822 Xia, F., Wang, J-G., Zhu, T., Zou, B., Rhee, S-K., and Quan, Z-X. (2018) Ubiquity and
823 diversity of complete ammonia oxidizers (commamox). *Appl Environ Microbiol* **84**:
824 e01390-18.
825 Yuan, Z., and VanBriesen, J.M. (2002) Yield prediction and stoichiometry of multi-step
826 biodegradation reactions involving oxygenation. *Biotechnol Bioeng* **80**: 100–113.
827 Zakem, E.J., Al-Haj, A., Church, M.J., van Dijken, G.L., Dutkiewicz, S., Foster, S.Q., et al.
828 (2018) Ecological control of nitrite in the upper ocean. *Nat Commun* **9**: 1206.
829 Zhang, Y., Qin, W., Hou, L., Zakem, E.J., Wan, X., Zhao, Z., et al. (2020) Nitrifier adaptation
830 to low energy flux controls inventory of reduced nitrogen in the dark ocean. *Proc Natl*
831 *Acad Sci U S A* **117**: 4823–4830.

832 **Table 1. Summary of metagenomic bins.** *Nitrospira*, *Nitrosomonas*, and *Nitrospina* bins

833 were designated with the label of "NPIRA", "NMNS", and "NPINA", respectively.

834 Phylogeny of the other DHS20C bins were shown in **Fig. S1**.

Bin(s)	Relative abundance (%)		Size (Mb)	Contigs	CDSs	Completeness	Contamination	Strain heterogeneity
	NH_4^+-enriched	NO_2^--enriched						
NPIRA01	1.44	39.7	4.7	203	4,095	90%	3%	50
NPIRA02	35.0	21.2	4.7	92	4,275	97%	3%	33
NPIRA03	1.08	1.50	4.9	218	4,203	94%	4%	20
NPIRA04	14.1	8.88	4.8	633	3,683	81%	4%	30
NPIRA05	0.59	0.73	3.1	595	2,336	59%	0%	0
NPIRA06	1.52	0.21	4.0	303	3,436	85%	5%	57
NMNS01	1.72	0.58	3.7	199	3,093	98%	1%	0
NMNS02	5.86	0.04	3.6	117	3,117	99%	2%	0
NPINA01	0.13	2.10	3.6	14	3,355	97%	3%	0
DHS20C01	1.01	0.73	4.4	119	3,859	99%	3%	8
DHS20C02	0.00	3.43	2.1	12	2,066	96%	1%	0
DHS20C03	1.47	0.51	4.6	234	4,050	100%	2%	82
DHS20C04	1.63	0.00	3.4	133	3,254	95%	0%	0

Bin(s)	Relative abundance (%)		Size (Mb)	Contigs	CDSs	Completeness	Contamination	Strain heterogeneity
	NH_4^+-enriched	NO_2^--enriched						
DHS20C05	0.43	0.00	3.0	386	2,588	84%	1%	17
DHS20C06	0.46	0.10	2.4	271	2,137	88%	0%	0
DHS20C07	2.79	0.07	3.6	27	3,178	100%	1%	0
DHS20C08	2.41	0.75	2.9	6	2,510	98%	1%	0
DHS20C09	0.46	0.07	2.8	420	2,257	84%	8%	3
DHS20C10	1.04	0.03	1.7	65	1,458	89%	1%	67
DHS20C11	0.00	0.81	4.7	210	3,873	96%	1%	0
DHS20C12	0.55	0.03	3.6	282	3,076	91%	11%	39
DHS20C13	1.01	0.14	3.4	173	3,114	97%	7%	9
DHS20C14	0.61	0.27	2.9	273	2,298	91%	3%	33
DHS20C15	1.41	0.03	4.5	11	3,500	96%	1%	0
DHS20C16	0.50	0.02	5.3	478	3,780	96%	9%	0
DHS20C17	0.46	0.19	5.2	462	3,634	97%	3%	0
DHS20C18	0.83	0.05	8.0	161	5,634	100%	1%	0
DHS20C19	0.44	0.17	3.7	589	3,085	80%	3%	0
DHS20C20	0.01	0.68	4.9	1044	3,440	73%	15%	70

Bin(s)	Relative abundance (%)		Size (Mb)	Contigs	CDSs	Completeness	Contamination	Strain heterogeneity
	NH_4^+-enriched	NO_2^--enriched						
DHS20C21	0.01	0.69	3.6	653	2,475	77%	4%	0

835

836 **Table 2 CO_2 assimilation and free-energy efficiencies of NH_4^+- and NO_2^--enriched**

837 **biomass, AOB, and NOB.** CO_2 assimilation efficiencies examining $^{14}CO_2$ fixation into

838 biomass during NH_3 or NO_2^- oxidation are summarized here, and the values are available as

839 (mean ± standard deviations). NA; not available because the NO_2^--enriched biomass did not

840 show the activity of aerobic ammonia oxidation. *; the value was calculated by subtracting the

841 CO_2 assimilation efficiency of aerobic ammonia oxidation with that of nitrite oxidation. The

842 CO_2 assimilation efficiencies in this table does not include a fraction of the carbon released as

843 dissolved organic carbon (DOC). The reference data of Bayer *et al.* (2022) are a personal gift

844 from Dr. Barbara Bayer.

Biomass/microorganisms	Reaction	μmol-CO_2/μmol-NH_3 or NO_2^- (Free-energy efficiency)	Reference
NH_4^+-enriched biomass	$NH_3 \rightarrow NO_3^-$	0.13 ± 0.019	this study
	$NH_3 \rightarrow NO_2^-$	0.077* (13%)	this study
	$NO_2^- \rightarrow NO_3^-$	0.053 ± 0.013 (31%)	this study
NO_2^--enriched biomass	$NH_3 \rightarrow NO_2^-$	NA	this study
	$NO_2^- \rightarrow NO_3^-$	0.054 ± 0.019 (32%)	this study
AOB			
Nitrosomonas marina	$NH_3 \rightarrow NO_2^-$	0.04 – 0.07 (7 – 12%)	Glover (1985)
Nitrosococcus oceanus	$NH_3 \rightarrow NO_2^-$	0.024 – 0.062 (4 – 11%)	Glover *et al.* (1985)
Nitrosomonas marina C-25	$NH_3 \rightarrow NO_2^-$	0.043 ± 0.012 (7%)	Bayer *et al.* (2022)

Biomass/microorganisms	Reaction	μmol-CO_2/μmol-NH_3 or NO_2^- (Free-energy efficiency)	Reference
Nitrosomonas sp. C-15	$NH_3 \rightarrow NO_2^-$	0.044 ± 0.007 (8%)	Bayer *et al.* (2022)
NOB			
Nitrococcus mobilis	$NO_2^- \rightarrow NO_3^-$	0.014 - 0.031 (9 – 21%)	Glover (1985)
Nitrococcus mobilis Nb-231	$NO_2^- \rightarrow NO_3^-$	0.016 ± 0.002 (11%)	Bayer *et al*., 2022
Nitrobacter agilis	$NO_2^- \rightarrow NO_3^-$	0.009 (6%)	Tsai and Tuovinen (1986)
Nitrospira marina Nb-295	$NO_2^- \rightarrow NO_3^-$	0.032 ± 0.005 (22%)	Bayer *et al*., 2022
Nitrospina sp. Nb-3	$NO_2^- \rightarrow NO_3^-$	0.035 ± 0.005 (23%)	Bayer *et al*., 2022
Nitrospina gracilis Nb-211	$NO_2^- \rightarrow NO_3^-$	0.029 ± 0.002 (19%)	Bayer *et al*., 2022

845

846 **Figure legends**

847 **Fig. 1. Fluorescence *in-situ* hybridization analysis of NH_4^+-enriched biomass.** The
848 biomass was fixed with 4% paraformaldehyde, hybridized with the oligonucleotide probe
849 Ntspa712 (labeled with Cy3) for *Nitrospira* (panel **a**) or Nsm156 (TRITC) for *Nitrosomonas*
850 (panel **b**), and stained with DAPI. The cells showing red and cyan color represent *Nitrospira*
851 or *Nitrosomonas* population (red) and total cells (cyan), respectively. Bar = 20 μm.

852 **Fig. 2. Genome tree showing the phylogeny of *Nitrospira* bins.** A phylogenetic clade of
853 *Nitrospira* sublineage IV was shown with a bracket, and the phylogenetic position of the
854 obtained *Nitrospira* bins affiliated into *Nitrospira marina* and *Nitrospira salsa* clades were
855 shown with red color. The scale bar represents 10% sequence divergence.

856 **Fig. 3. Genome tree showing the phylogeny of *Nitrosomonas* bins.** The phylogenetic
857 position of the obtained *Nitrosomonas* bins were shown with red color. The scale bar
858 represents 5% sequence divergence.

859 **Fig. 4. Nitrification activities of NH_4^+- and NO_2^--enriched biomass (left and right panels,**
860 **respectively)**. The biomass was aerobically incubated with the addition of NH_4^+ or NO_2^-, and
861 the concentrations of NH_4^+, NO_2^-, and NO_3^- were determined. The incubation was performed
862 in triplicates, and the symbol and error bars represent the mean value and the range of
863 standard deviation, respectively.

864 **Fig. 5. Aerobic H_2 oxidation by NH_4^+- and NO_2^--enriched biomass.** The biomass

865 suspension (2.5 mL) was incubated in closed 10-mL vials with the addition of pure H_2 gas

866 into the head space, and the concentrations of H_2 and O_2 in the head space were monitored.

867 Both the biomass consumed H_2, while the consumption required more than 4 d of lag phase.

868 Error bars represent the range of standard deviation derived from triplicate incubations.

869 **Fig. 6. Abundance of AOB and *Nitrospira* in the NH_4^+-enriched biomass and the reactor**

870 **effluents discharged from the NH_4^+-feeding DHS reactor.** Copy numbers of bacterial 16S

871 rRNA gene, AOB *amoA*, *Nitrospira nxrB*, and *Nitrospira* 16S rRNA gene were determined

872 by quantitative PCR assay. Genomic DNA extraction was performed with >3 biomass

873 samples, and error bar represent the standard deviation of the copy numbers determined from

874 each DNA extracts.

a)

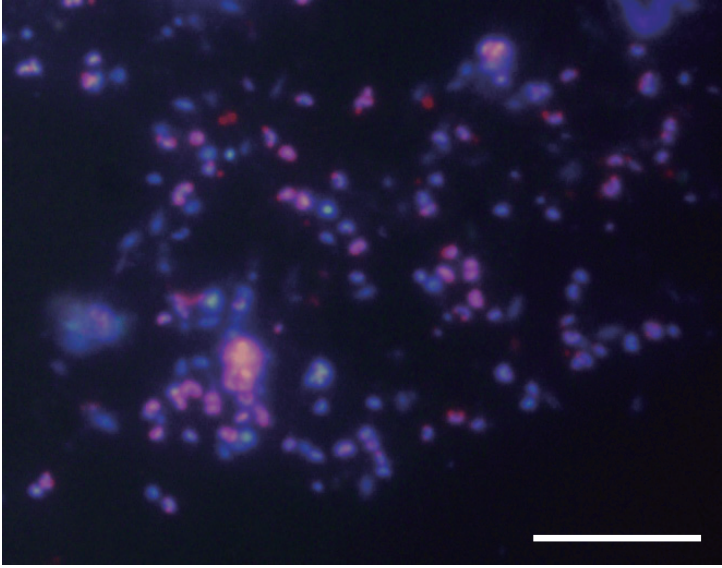

b)

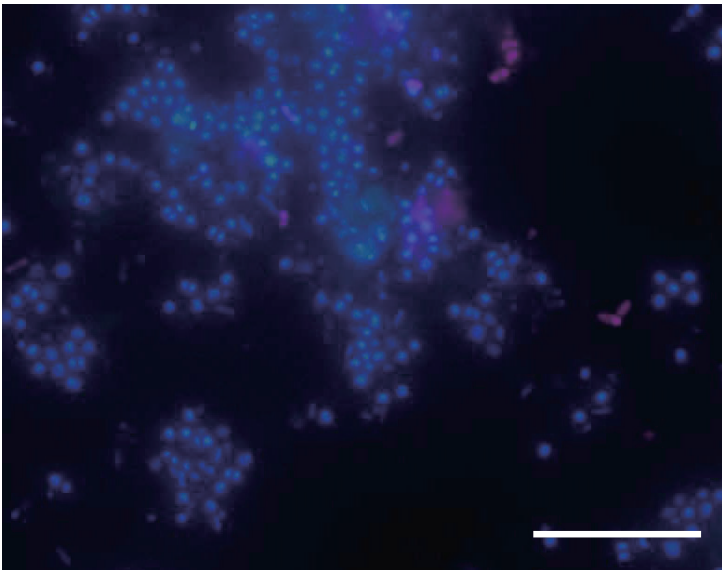

Fig. 1 (Oshiki et al.)

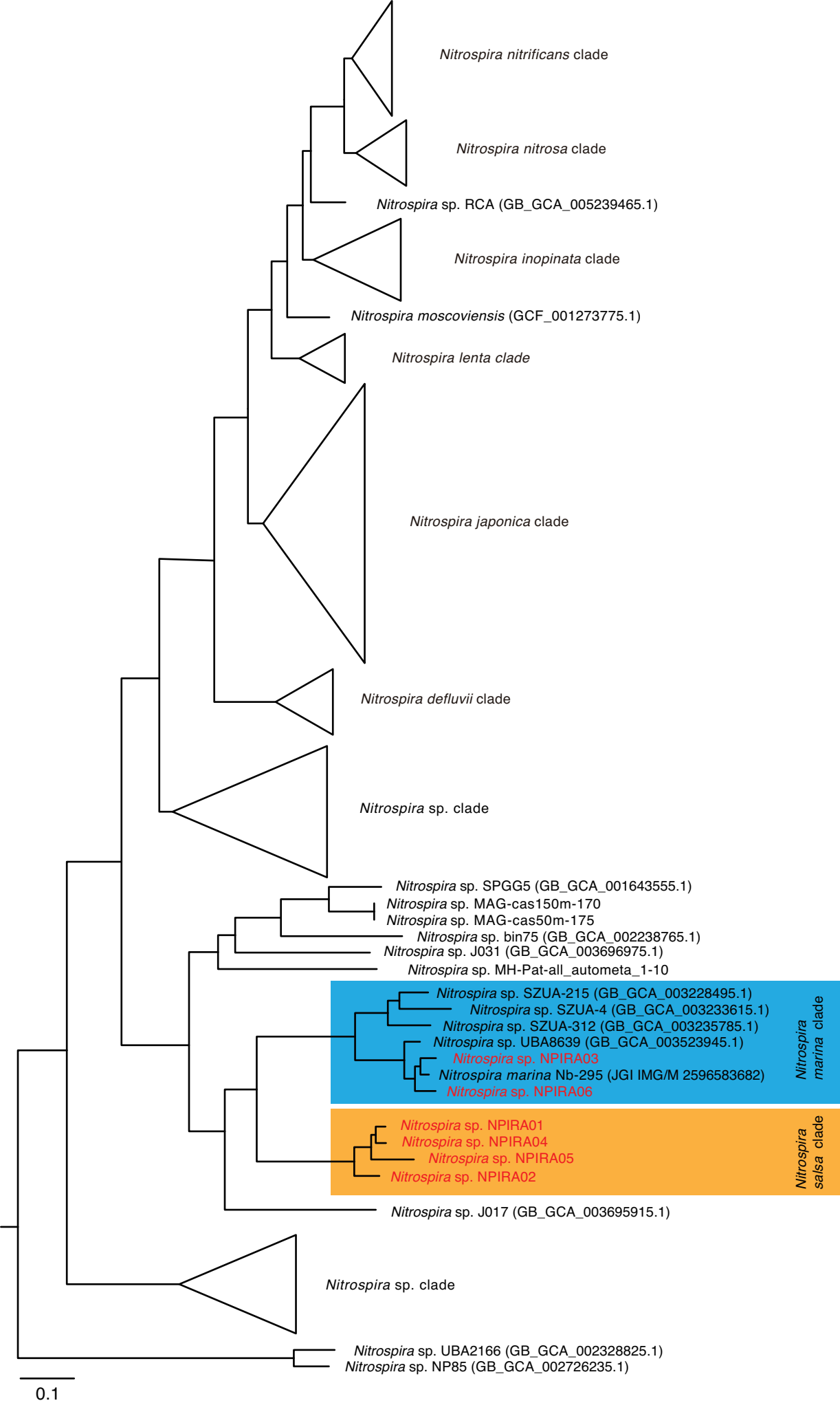

Fig. 2 (Oshiki et al.)

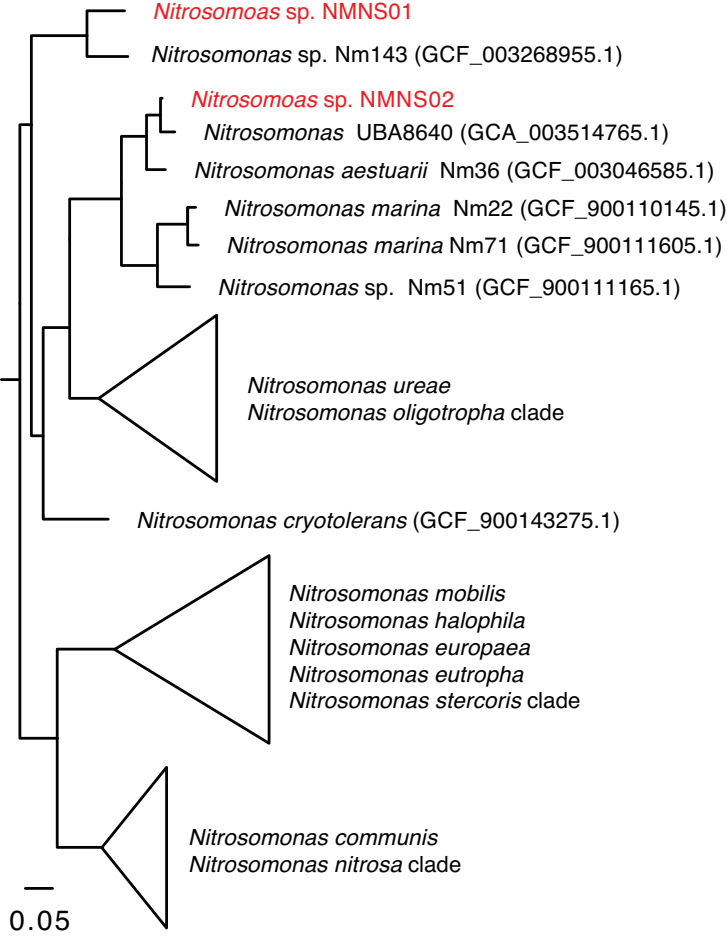

Fig. 3 (Oshiki et al.)

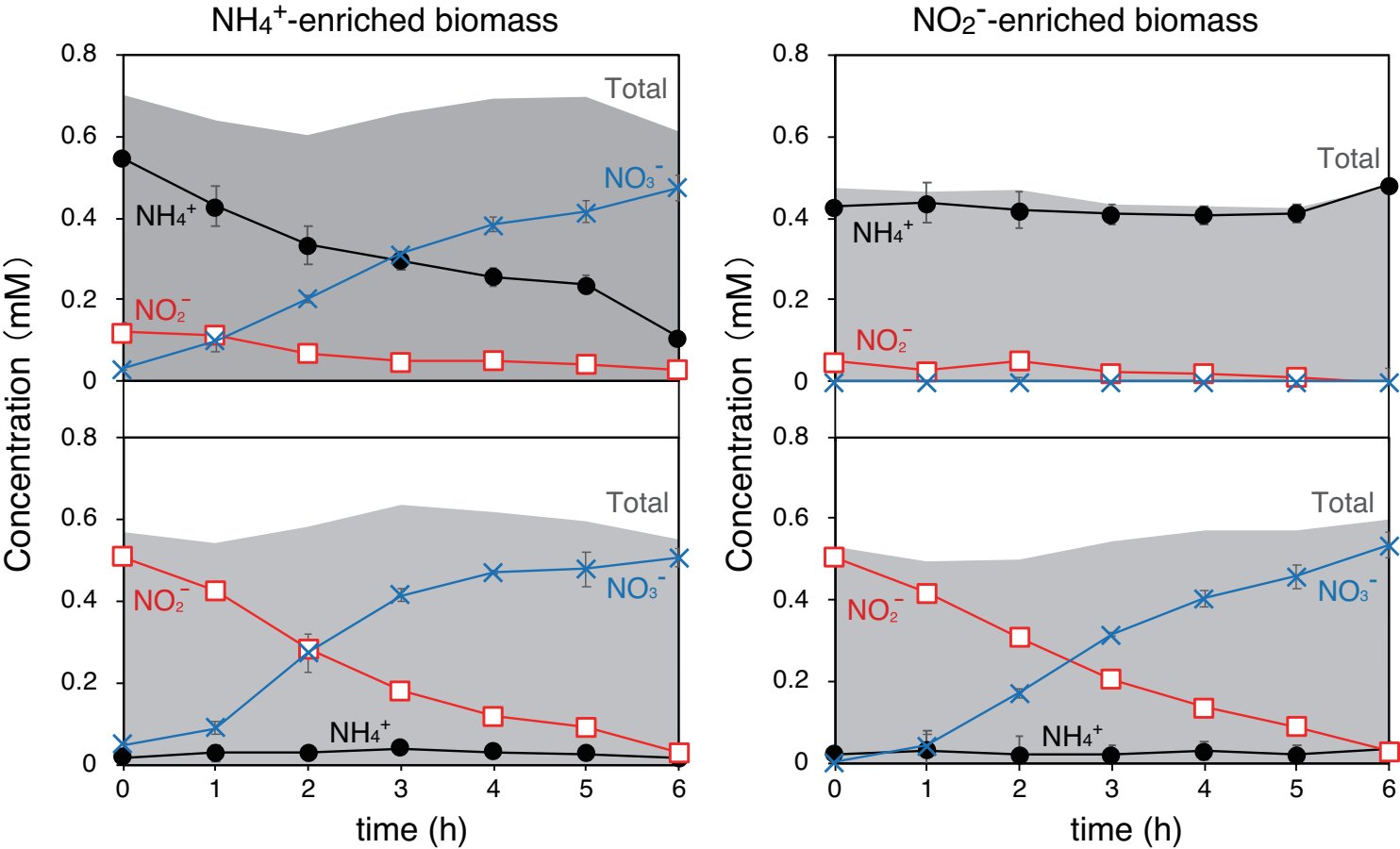

Fig. 4 (Oshiki et al.)

a) NH_4^+-enriched biomass

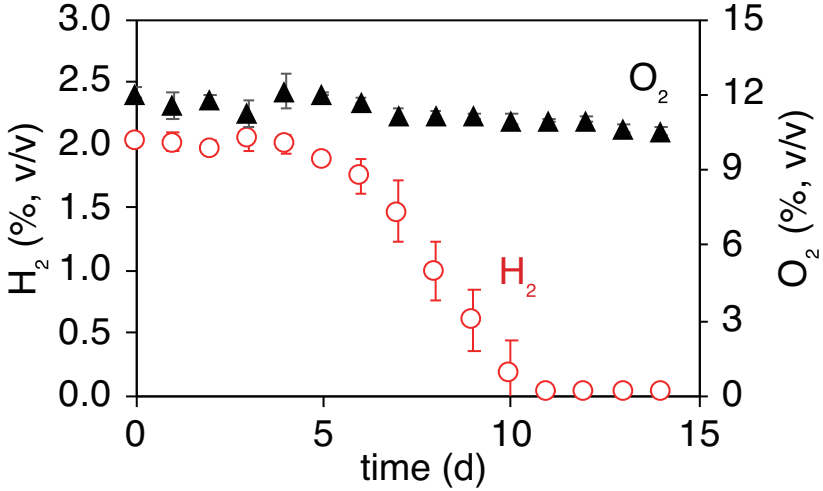

b) NO_2^--enriched biomass

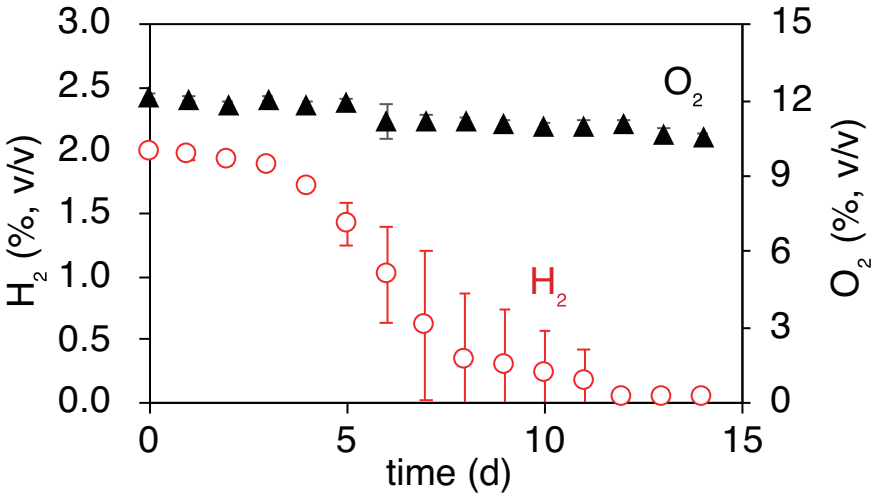

Fig. 5 (Oshiki et al.)

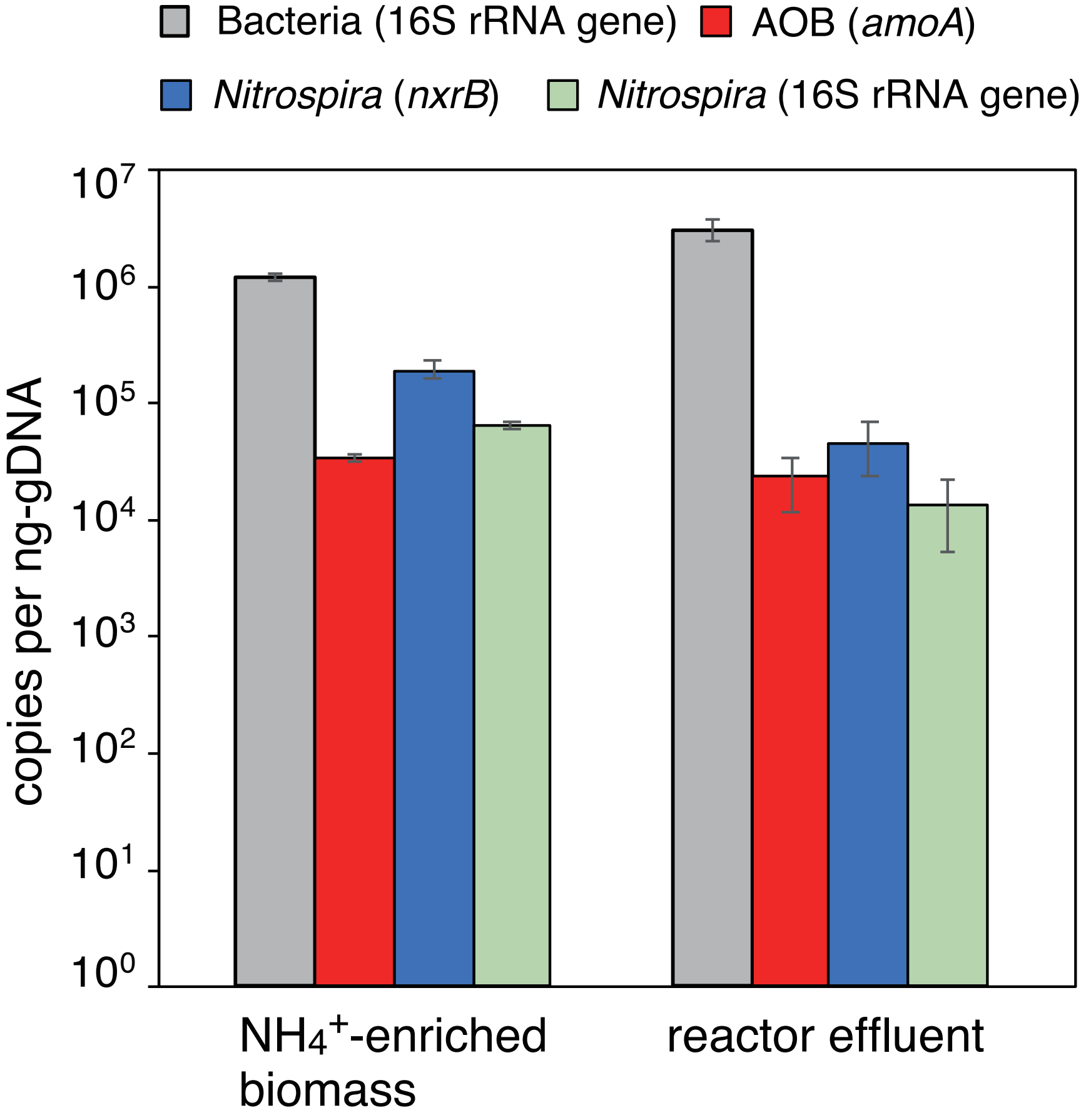

Fig. 6 (Oshiki et al.)